

AD-A264 517



(2)

2

MEASUREMENT OF THE MAGNETIC AND ELECTRICAL ACTIVITY  
OF INDIVIDUAL CELLS IN VITRO

FINAL REPORT

CHRISTOPHER C. DAVIS

FEBRUARY 26, 1993

Supported by

U.S. ARMY MEDICAL RESEARCH AND DEVELOPMENT COMMAND  
Fort Detrick, Frederick, Maryland 21702-5012

Grant No. DAMD17-90-Z-0052

University of Maryland  
Electrical Engineering Department  
College Park, Maryland 20742

Approved for public release; distribution unlimited.

The findings in this report are not to be construed as an  
official Department of the Army position unless so designated  
by other authorized documents

**93 5 18 04 6**

**93-11085** 9208

**DTIC**  
**S** **ELECTE** **D**  
**MAY 19 1993**  
**C**

# REPORT DOCUMENTATION PAGE

Form Approved

OMB No 0704-0188

Public reporting burden for this collection of information is estimated to average 1 hour per response, including the time for reviewing instructions, searching existing data sources, gathering and maintaining the data needed, and completing and reviewing the collection of information. Send comments regarding this burden estimate or any other aspect of this collection of information, including suggestions for reducing this burden, to Washington Headquarters Services, Directorate for Information Operations and Reports, 1215 Jefferson Davis Highway, Suite 1204, Arlington, VA 22202-4302 and to the Office of Management and Budget, Paperwork Reduction Project (0704-0188), Washington, DC 20503

1. AGENCY USE ONLY (Leave blank)

2. REPORT DATE

Feb. 26, 1993

3. REPORT TYPE AND DATES COVERED

Final 24 Sep 90 - 23 Sep 92

4. TITLE AND SUBTITLE

Measurement of the Magnetic and Electrical Activity of Individual Cells In Vitro

5. FUNDING NUMBERS

DAMD17-90-Z-0052  
61102A  
30161102BS15 CE  
DA335569

6. AUTHOR(S)

Christopher C. Davis

7. PERFORMING ORGANIZATION NAME(S) AND ADDRESS(ES)

University of Maryland  
Electrical Engineering Department  
College Park, Maryland 20742

8. PERFORMING ORGANIZATION REPORT NUMBER

9. SPONSORING / MONITORING AGENCY NAME(S) AND ADDRESS(ES)

U.S. Army Medical Research & Development Command  
Fort Detrick  
Frederick, Maryland 21702-5012

10. SPONSORING / MONITORING AGENCY REPORT NUMBER

11. SUPPLEMENTARY NOTES

12a. DISTRIBUTION / AVAILABILITY STATEMENT

Approved for public release;  
Distribution unlimited

12b. DISTRIBUTION CODE

13. ABSTRACT (Maximum 200 words)

This report describes the development of both incoherent and coherent fiber optic sensors for monitoring the electrical activity of cells and tissue. The incoherent sensors use an optical fiber to deliver laser light to a cell membrane that is stained with a voltage-sensitive dye. The change in resulting fluorescence allows the electrical activity of the cell to be monitored. The coherent fiber sensor uses an external element, either a cell or some other material that has induced birefringence, as an extrinsic sensing element. The fiber is a means for delivering coherent light to this element. Birefringence-induced phase changes are detected in a heterodyne interferometric scheme. This report also describes the development work to date on NanoSQUID, a very small scale, superconducting quantum interference device that will allow spatially-resolved measurements of the magnetic activity of cells and tissue.

14. SUBJECT TERMS

Fiber optic sensors; SQUID magnetometers;  
Voltage-sensitive dyes; Cellular electrical activity;  
RA 3

15. NUMBER OF PAGES

16. PRICE CODE

17. SECURITY CLASSIFICATION OF REPORT

Unclassified

18. SECURITY CLASSIFICATION OF THIS PAGE

Unclassified

19. SECURITY CLASSIFICATION OF ABSTRACT

Unclassified

20. LIMITATION OF ABSTRACT

Unlimited

## CONTENTS

Summary	1
Extrinsic Optical Heterodyne Fiber Sensor	1
Work to date on NanoSQUID	3
Cellular Magnetic Fields	4
Circulating Ion Currents on the Membrane	5
SQUID Operation	5
Introduction to Coherent Sensor Technology	6
Operating Principles of Coherent Sensors	7
Studies of Cell Electrical Activity from Membrane Birefringence	10
Heterodyne Fiber Sensors	11
New Heterodyne Fiber Sensors	12
High Resolution Imaging	14
References	15
Appendices	18

DTIC QUALITY INSPECTED 5

Accession For	
NTIS CRA&I	<input checked="checked" type="checkbox"/>
DTIC TAB	<input type="checkbox"/>
Unannounced	<input type="checkbox"/>
Justification	
By	
Distribution /	
Availability Codes	
Dist	Avail and/or Special
A-1	

## SUMMARY

This final report has two parts. The first part describes the development of a common-path, optical heterodyne fiber sensor for remote monitoring of the electrically induced birefringence of materials. The second part is a report from Professor John P. Wikswo of Vanderbilt University, who is a sub-contractor on the University of Maryland contract. He is working on the development of a very small SQUID "NanoSQUID", which will allow monitoring of the magnetic fields from cells and tissues within about 2mm of tissue at physiological temperature. The SQUID is at  $\sim 4K$ .

## EXTRINSIC OPTICAL HETERODYNE FIBER SENSOR

The principle of this sensor is that an electrooptically active medium placed at the end of the sensor will induce a differential phase shift between two offset laser frequencies propagating in the fiber. Since the fiber is only a means of delivering laser light to the sensor element, which will eventually be a cell, the sensor is referred to as "extrinsic." In application of this sensor to a study of cellular electrical activity the fiber sensor observes changes in cell membrane birefringence. In this sense the cell becomes the "extrinsic" sensor element.

In parallel with our development of a coherent sensor of cellular electrical activity we have been continuing work on an incoherent fiber optic probe of the same phenomenon. We have had considerable success already with these incoherent fiber optic probes that utilize voltage-sensitive dyes bound to the cell membrane [1,2]. Two of the publications that describe this work are appended to this report. This work was done in conjunction with scientists from the FDA Center for Devices and Radiological health in Rockville, Maryland.

The coherent sensor uses the naturally varying birefringence of the cell membrane that occurs during polarization and depolarization as an extrinsic sensor element. Research on this sensor is well advanced and it has been successfully implemented in several non-biological experiments. To optimize the performance of the sensor it has proven easiest to build various versions and test them in situations where birefringence can be induced and the sensor can be optimized. In a series of papers we have demonstrated that a heterodyne

version of this sensor can detect birefringence effects at the distal end of the sensor  $\sim 1\mu\text{rad}$ . This sensitivity should be adequate for the study of cell membranes where birefringence effects of about  $1\text{mrad}$  have been observed in transmission.

Our successes to date with our coherent, hybrid, extrinsic fiber sensors – so called because the single-mode fiber serves as a delivery pathway for coherent light to a sensor element at the distal end of the fiber – have been spectacular. Not only can we see weak induced birefringence produced by both electric and magnetic fields, we can monitor mechanical motions on the order of picometers at the end of the fiber. These observations can be made in a spatially resolved way with  $\sim 0.5\mu\text{m}$  resolution. It turns out that delivering light from a fiber to a sample followed by collection of the light by the same fiber, gives a confocal-type resolution advantage. We are in the process of exploiting this further by making tapered fiber tips and using the emerging techniques of near-field optical microscopy to achieve resolutions that should ultimately reach into the nanometer region. In summary: highlights of our work to date are:

- remote detection of induced birefringence with microradian sensitivity
- use of a coherent, hybrid extrinsic sensor to perform spatially resolved imaging on GaAs circuits – used by us as a convenient test vehicle that is easier to handle during optimization than cells *in vivo* or *in vitro*.
- surface imaging in three-dimensions with  $\sim 0.5\mu\text{m}$  resolution
- development of tapered fiber tips with size  $< 100\text{nm}$ , which should allow increased resolution.

These developments are well described in the reprints and preprints that are appended to this report. These developments in the use of scanning fiber probes for sub-micrometer imaging are potentially more exciting even than the use of the probe for electrical field measurements. In contrast to Scanning Tunneling Microscopes (STMs), and to some extent Atomic Force Microscopes (AFMs), the emerging field of Scanning Tunneling Optical Microscopy (STOM) can provide imagery of live biological materials. A conductive, dead, metal-coated sample is not required.

## WORK TO DATE ON NanoSQUID

Substantial effort has been directed towards the optimization of the SQUID sensors required for nanoSQUID. Initially, Professor Wikswo intended to utilize miniature pickup coils connected to separate DC SQUID sensors, but came to recognize that there would be severe problems with impedance matching and stray pickup in coupling the low inductance pickup coils to the existing high inductance SQUID sensors. Claudia Tesche and Mark Ketchen of IBM then agreed to fabricate a custom SQUID sensor with an integral, miniature gradiometer, so that the low inductance pickup coil could be properly matched to a low inductance SQUID. He then conducted an extensive design study to devise the optimum coil geometry, and Claudia Tesche prepared the circuit layout. Process problems at IBM prevented the successful fabrication of the devices using 0.5 micron Josephson junctions and circuit linewidths, so the circuits were then modified to use larger junctions and one micron linewidths. The modified circuits are presently being processed and should be available in the near future.

In parallel with this effort, he has continued to develop the cryogenic instrumentation required for nanoSQUID. He has obtained a set of state-of-the-art, four-channel SQUID electronics from Quantum Design. Preliminary tests of the SQUID sensors will be conducted in a probe that has been developed for immersion in a liquid helium storage dewar, and subsequently the sensors will be mounted in a novel cryogenic refrigerator that was custom-fabricated by Abbess Instruments to provide the small pickup-coil to sample distance.

The development of high resolution SQUID magnetometers poses a number of challenging technical problems, but these instruments will be unique in their ability to measure quantitatively action currents at the cellular level. While electrical measurements of biological systems have been explored extensively over the past century, only in the past few years has it been possible to utilize magnetic measurements to image cellular action currents. Many biological phenomena, particularly those involving cell-to-cell communication and non-uniform propagation, are governed by the transfer of electrical charge. Since the distributed electrical resistivity and capacitance of these systems is often unknown or poorly

characterized, electrical measurements alone cannot suffice to quantify this charge transfer. Hence direct measurements of current are crucial to understanding cell-to-cell coupling. More importantly, the combination of magnetic measurements of current and electrical and optical measurements of voltage offers unique promise towards improving our understanding of not only the transfer of charge between cells but also the tissue properties that relate current to voltage.

## CELLULAR MAGNETIC FIELDS

Although the magnetic activity of large organs of the human body has been frequently observed [3-16], and indeed has been used for diagnostic purposes in a clinical setting [5,8,15], the magnetic activity of individual cells has never, to the best of our knowledge, been observed. These fields are expected to be small, as the fields produced by large organs are themselves quite small. For example the fields generated by a healthy heart are on the order of 50pT ( $10^{-8}$  Gauss) when monitored close to the chest, magnetic contaminants in the lung can lead to nearby fields of 100pT, the brain alpha rhythm produces about 1pT, and the brain activity evoked by sensory stimuli is on the order of 0.1pT [13]. Larger magnetic fields are generated by the current flow in single axons. Wikswo and co-workers [17] have demonstrated that they can be detected with a ferrite core toroidal transformer and special amplifier system [18,19]. The magnetic field from medial giant axons changes by 200pT in 0.1ms.

The magnetic fields associated with single cells, or small groups of cells, are expected to be very small, particularly if the electrical activity of the cell only involves a few ion channels in the membrane. However, electrically active cells involve many channels and combined channel activity can easily reach  $10\mu\text{A}$  for a cell about  $100\mu\text{m}$  in diameter [20], as has been observed, for example, in squid (the marine variety) giant axons. Heart cells, which are very active electrical, probably involve cellular currents up to  $10\mu\text{A}$ . Such a trans-membrane current could lead to a flux linkage of  $3.75 \times 10^{-5}$  fluxon. This lies within the detection capability of SQUID magnetometers, which have achieved performance on the order of  $10^{-6}$  fluxon /  $\sqrt{\text{Hz}}$  [21,22].

## **CIRCULATING ION CURRENTS ON THE MEMBRANE**

If ion currents circulate near, or on, the membrane, larger magnetic fields may be generated, flux linkages through an external coil might easily be several fluxon or larger. Certainly, if such currents exist their detection will be much more straightforward than if only transmembrane currents are to be detected.

## **SQUID OPERATION**

The basic theory underlying the operation of a DC SQUID has been given in several references [23-25] so we will not review it further here.

The following section provides a detailed, tutorial discussion of the underlying principles of coherent optical sensors. It is provided for the reader who is not acquainted with these ultra-sensitive devices.

## **INTRODUCTION TO COHERENT SENSIR TECHNOLOGY**

Coherent optical sensors utilize homodyne or heterodyne interferometry to detect small phase modulations or chirps impressed on a single frequency laser beam by the phenomenon being sensed. In some sensors that we have developed for magneto-optical studies, the optical mixing occurs between two orthogonal polarization states of a beam that are modified by a magneto-nonlinear sample and recombined with a polarization sensitive beam splitter. Coherent sensors that are well designed and fabricated work at the photon noise limit.

The technological development of coherent sensors for practical applications requires that the sensor be:

- easy to use
- very sensitive in the required application
- have wide dynamic range
- have sufficient bandwidth

For biological sensing applications, in addition it is desirable that the sensor be:

- minimally invasive
- biocompatible
- have resolution on a micrometer size scale

For detection of the electrical activity of individual cells it is also important that the sensor not perturb the natural field associated with the cell.

To accomplish these goals we have developed fiber optic probes that can be used to monitor local changes in birefringence that occur in a medium placed at the end of the fiber. The single mode fiber in all these experiments serves as a delivery system for coherent light that is modified by the medium, or media, placed at the end of the fiber. The modification of the light appears as a phase, or polarization modulation of the light returned down

the fiber. The phenomenon is studied by demodulating this FM or PM signal containing the sensor information desired. The exact demodulation scheme used depends on the sort of phenomenon being sensed. Low frequency, thermal phenomena are best studied directly in base-band by using homodyne techniques, while other coherent probes utilize true heterodyne techniques to extract the information required and avoid the system phase stabilization needed in the homodyne sensors. We are working on several different demodulation schemes involving highly linear discriminators, phase-locked loops, and direct digital data acquisition and tracking.

## OPERATING PRINCIPLES OF COHERENT SENSORS

Before describing the value of fiber sensors as a means for studying the electrical activity of individual cells *in vitro* we will review the use of laser homodyne (or heterodyne) interferometry as a sensor technique. This can best be done with reference to the archetypal experimental arrangement shown in Fig. (1).

A single-frequency laser beam illuminates a Mach-Zehnder interferometer, one arm of which contains a sample whose refractive index is modified by some physical phenomenon - for example the application of an electrical or magnetic field. The electric field of the wave that has passed through the sample can be represented at detector 1 by its analytic signal as

$$E_S = E_A e^{i(\omega t + \phi_A + \Delta\phi(t))}, \quad (1b)$$

where  $\phi_A$  is a static phase factor and  $\Delta\phi(t)$  is an induced phase chirp. For a uniform change in index along the path

$$\Delta\phi(t) = \frac{2\pi\ell n(t)}{\lambda_0} \quad (2b)$$

If the change in index is a function of position along the path then

$$\Delta\phi(t) = \frac{2\pi}{\lambda} \int_0^{\ell} n(x, t) dx \quad (3b)$$

The electric field of the reference wave can be similarly represented as

$$E_R = E_B e^{i(\omega t + \phi_B)}. \quad (4b)$$

If detector 1 is a square law detector its output is

$$\begin{aligned} i_1(t) &\propto (E_S + E_R)^*(E_S + E_R) \\ &\propto E_A^2 + E_B^2 + 2E_A E_B \cos(\phi_A - \phi_B + \Delta\phi(t)) \\ &\propto E_A^2 + E_B^2 + 2E_A E_B \cos(\phi_A + \phi_B) - 2E_A E_B \sin(\phi_A - \phi_B) \Delta\phi(t) \end{aligned} \quad (5b)$$

where we have used the small-angle approximation. Optimum demodulation occurs if

$$(\phi_A - \phi_B) = (2n + 1)\pi/2. \quad (6b)$$

Since the total intensity passing to detectors 1 and 2 is constant, it is easy to see that the output from detector 2 is

$$i_2(t) \propto E_A^2 + E_B^2 - 2E_A E_B \cos(\phi_A - \phi_B) + 2E_A E_B \sin(\phi_A - \phi_B) \Delta\phi(t). \quad (7b)$$

Note that if  $E_A = E_B$  then  $E_A^2 \propto I/4$  where  $I$  is the laser power. If  $\Delta\phi(t)$  is sinusoidal and is written in the form

$$\Delta\phi(t) = -m \sin \omega_m t, \quad (8b)$$

where  $m$  is called the depth of modulation, then the wave emerging from the sample cell is a phase modulated wave with Bessel-function-amplitude sidebands at frequencies  $\omega \pm p\omega_m$  where  $p$  is an integer. For small modulation depths  $m \ll 1$  the only sidebands of importance are at  $\omega \pm \omega_m$ . Their amplitudes are  $J_1(m)$  relative to the carrier whose amplitude is  $J_0(m)$ . The demodulation process involves detection of these sidebands. For coherent detection (which is true in this case as both signal and reference waves are derived from the same laser) the signal to noise ratio is [33]

$$\frac{S}{N} = \frac{\eta P_s}{h\nu \Delta f}, \quad (9b)$$

where  $P_s$  is the power associated with **both** sidebands,  $\eta$  is the quantum efficiency of the detector,  $h\nu$  is the quantum energy from the laser and  $\Delta f$  is the signal processing bandwidth.\* If

$$m = \frac{4\pi\ell\Delta n}{\lambda_0}, \quad (10b)$$

which corresponds to sinusoidal refractive index modulation of amplitude  $\Delta n$ , then the sideband power is

$$P_s = \frac{aPm^2}{4} = \frac{4\pi^2\ell^2 aP(\Delta n)^2}{\lambda_0^2}, \quad (11b)$$

where

$$a = \frac{E_A^2}{E_A^2 + E_B^2} \quad (12b)$$

and  $P$  is the total laser power.

The coefficient  $a$  is determined by the effective reflectance/transmittance of the first beam splitter in Fig. (1). Usually  $a \simeq 1/2$ .

Thus for a  $S/N = 1$

$$\Delta n_{\min} = \frac{\lambda_0}{2\pi\ell} \left( \frac{h\nu\Delta f}{a\eta P} \right)^{1/2}. \quad (13b)$$

For  $\lambda_0 = 514.5nm$ ,  $a = 0.5$   $\eta = 0.85$  this translates into a minimum refractive index modulation of

$$\Delta n_{\min} = 2.5 \times 10^{-13} / \sqrt{Hz/cm} / \sqrt{mW}. \quad (14b)$$

We and others have achieved sensitivities of this order in practice.

---

\* The  $S/N$  ratio predicted by Eq. (9b) can be reduced by up to a factor of 2 depending on the specific detection mechanism in the photodetector[34]

In practice it is difficult to approach sensitivities near the photon-noise limit predicted by Eq. (14b) without compensating for amplitude noise from the source laser. It is also desirable, if possible, to use a single frequency laser in these experiments to eliminate noise resulting from modulation of intermode beat signals. The best way to virtually eliminate amplitude noise problems in experiments of this sort is to use a balanced optical mixer. This is not a new idea, indeed it parallels closely the balanced microwave mixer first described by Dicke [35] in 1946. A recent quantum-mechanical analysis of the noise reduction properties of this detection scheme has been given by Yuen and Chan [36]. In a 2-detector scheme as shown in Fig. (1), if the average signal levels from detector 1 and 2 are made equal and then subtracted, a substantial part, but not all [37] of the AM noise is removed. The result obtained if

$$(\phi_A - \phi_B) = (2n + 1)\pi/2 \quad (15b)$$

is

$$i_2(t) - i_1(t) \propto 4E_A E_B \Delta\phi(t). \quad (16b)$$

The phase modulation  $\Delta\phi(t)$  is thereby detected in the optimum way. This technique also ensures that all the sideband power is detected, which is not true in a single detector device.

In a heterodyne coherent sensor, one of the beams in Fig. (1) is frequency shifted with an acoustooptical modulator. The sensor information must then be extracted from the phase-modulated beat signal at the acoustooptical modulator offset frequency. This method of operation is more complex from a signal processing standpoint than the homodyne scheme and has only half the signal-to-noise ratio. However, it has the significant advantage of requiring no phase stabilization to preserve linear response: all that is needed to accomplish this is a highly linear discriminator or phase-locked loop demodulator.

## **STUDIES OF CELL ELECTRICAL ACTIVITY FROM MEMBRANE BIREFRINGENCE**

If a laser beam is directed down a single-mode fiber that is placed almost against a cell membrane *in vitro* then a sizable fraction of the emerging light will make a double pass

through the membrane and be recollected by the fiber. The electrical activity of the membrane will show up as a modulation of the polarization state of the returning light. Cell membranes are known to be electrooptically active in this way [38]. This polarization modulation can also be regarded as a phase retardation between the two orthogonal polarization components of the returning beam. The phase retardation can be written in the form

$$\Delta\phi = \frac{2\pi n^3 r V}{\lambda}, \quad (1c)$$

where  $\lambda$  is the laser wavelength,  $n$  is the refractive index of the membrane, and  $V$  is the voltage across the membrane [34]. With  $V=100\text{mV}$ ,  $\lambda=632.8\text{nm}$ ,  $n=2$ , and taking  $r=10^{-10} \text{ m/V}$ , which is a reasonable value for a fairly electrooptically active material, the phase retardation is  $0.8\text{mrad}$ . This is a relatively large value. We have previous experience in constructing sensors with sensitivity  $\sim 10^{-7} \text{ rad}/\sqrt{\text{Hz}}$ . We plan to modify one of our existing sensor systems to allow us to study the electrical activity of single cells in this way. The following sections of this report will give some details of how this will be done, and includes a tutorial discussion of fiber sensors in general. The two principal advantages of this approach are that it is non-invasive, very sensitive, and allows spatial resolution on a scale of  $\sim 1\mu\text{m}$  of the electrical activity at different points of the membrane surface.

## HETERODYNE FIBER SENSORS

Fiber sensors come in both incoherent [1,2] and coherent forms [39,40]. We are interested in the former as a means for studying cell activity through the emission of special dye molecules whose fluorescence spectrum varies as a function of the trans-membrane potential. We are working on coherent heterodyne fiber sensors for local probing of birefringence in cell membranes induced by the local trans-membrane electric field. These sensors are being studied in several configurations, using conventional and polarization preserving single-mode fibers. An ideal all-fiber sensor of this kind would include fiber splitters and in-fiber frequency shifting. From a practical standpoint, however, the technology to build such a system is not quite mature, so we are using external frequency shifting with acoustooptical modulators, and hybrid free-space/fiber interferometers.

## NEW HETERODYNE FIBER SENSORS

Homodyne interferometric sensors suffer from a phase ambiguity because both sidebands of a sinusoidal component of an induced phase chirp are symmetrically placed. However, heterodyne sensors do not suffer from this disadvantage, although their use involves an extra degree of complexity in signal demodulation. The use of FM (or PM) demodulation techniques that are standard in conventional FM receiver design allows the use of heterodyne techniques in many sensor applications. The principal difference between FM sensor demodulation and conventional FM demodulation revolves around:

- large modulation depths in one frequency band may need to be handled in the presence of small modulation depths in a second frequency band. This requires the development of sophisticated, highly linear, broadband FM discriminators, or the use of high order phase-locked loop techniques. We have investigated both approaches.
- for the detection of very weak phenomena the phase modulations or chirps that must be detected can be tiny: for example  $< 10^{-7} \text{ rad}/\sqrt{\text{Hz}}$ . In applications where the phenomena produce phase modulations at low frequencies, the demodulation of a small modulation at a low frequency on a much larger frequency IF represents a serious challenge. Homodyne techniques may still be preferable in such applications, for example in photothermal spectroscopy and low frequency magneto-optical studies.

Ref.[40] provides a good description of the sensor scheme that we have found most satisfactory so far for remote detection of induced birefringence. The beam from a single-frequency laser is split and one part is frequency shifted by an acoustooptical modulator, typical frequency offsets that we use are  $\sim 40\text{MHz}$ . The two beams are orthogonally polarized by sending one through a  $\lambda/2$  plate and are then directed into a single-mode fiber. At the end of the fiber the two orthogonal polarizations interact with an electro-optical or magneto-optic element, reflect, and return back along the fiber. A fiber coupler directs part of each polarization state into a balanced mixer. The balanced mixer is constructed from a polarizing beam splitter set at an appropriate angle (usually  $45^\circ$ ) to the original orthogonal polarization directions.

We can represent the electric field of the injected vertical polarization after the modulator

as

$$E_1 = E_0 \cos(\omega_0 t + \phi_0), \quad (1d)$$

and the horizontal polarization as

$$E_2 = E_0 \cos((\omega_0 + \omega_1)t + \phi_1). \quad (2d)$$

To simplify the discussion equal beam intensities are assumed. In the application of single-mode fibers to the study of cell membrane birefringence the length of fiber needed to deliver the beam to the cell to be probed is short, so we will neglect the birefringence of the fiber, although such birefringence can be dealt with. After returning through the membrane the vertical polarization can be represented as

$$E_1 = rE_0 \cos(\omega_0 t + \phi_0 + \phi_v). \quad (3d)$$

The horizontal component is

$$E_2 = rE_0 \cos((\omega_0 + \omega_1)t + \phi_1 + \phi_h), \quad (4d)$$

where we are for simplicity assuming equal amplitude reflection coefficients for the two polarizations. The two polarizations are partitioned at the polarizing beam-splitter and give photodiode currents

$$i_a \propto |E_1|^2,$$

and

$$i_b \propto |E_2|^2.$$

The result of the detection process is:

$$i_a \propto E_0^2 + E_0^2 \cos(\omega_1 t + \phi_x - \phi_y) \quad (5d)$$

$$i_b \propto E_0^2 - E_0^2 \cos(\omega_1 t + \phi_x - \phi_y), \quad (6d)$$

where  $\phi_x = \phi_1 + \phi_v$  and  $\phi_y = \phi_2 + \phi_h$ . Balanced mixing removes common mode noise ( amplitude fluctuations) to give:

$$i_a - i_b = 2E_0^2 \cos(\omega_1 t + \phi_x - \phi_y), \quad (7d)$$

which can be expanded to give

$$i_a - i_b = 2E_0^2[\cos(\omega_1 t + \phi_v - \phi_h) \cos(\phi_1 - \phi_2) + \sin(\omega_1 t + \phi_v - \phi_h) \sin(\phi_1 - \phi_2)]. \quad (8d)$$

The desired signal is the birefringence modulation  $\phi_v - \phi_h$ , which can be demodulated by conventional techniques.

## HIGH RESOLUTION IMAGING

We have been successful recently in using coherent fiber and free-space interferometric techniques to perform imaging of both three-dimensional features [41], and birefringence patterns in the surface of small structures [42]. This work, which has potentially enormous biological significance has been a spin-off of our work on the development of a fiber-optic probe for studying cellular electrical activity. The great advantage of this optical technique over scanning electron microscopy, scanning tunneling microscopy, and to some extent, atomic force microscopy, is that it can provide imagery of biological structures in the living state. These techniques are described in the papers appended to this report.

## REFERENCES

- [1] T.A. Bowmaster, C.C. Davis, and V. Krauthamer, "Excitation and Detection of Action Potential Induced Fluorescence Changes through a Single Monomode Optical Fiber," *Biochimica et Biophysica Acta*, 1091, 9-14, 1991
- [2] V. Krauthamer, H.J. Bryant, C.C. Davis, and T.W. Athey, "Action Potential Induced Fluorescence Changes Resolved with an Optical Fiber Carrying Excitation Light," to be published in the *Journal of Fluorescence*.
- [3] D. Cohen, *Physics Today*, August 1975
- [4] G.M. Baule and R. McFee, *Am. Heart J.*, 66,95,1963; and *J. Appl. Phys.*, 36,2066,1965
- [5] B. Denis, D. Matelin, C. Favier, M. Tanche, and P. Martin-Noel, *Arch. Mal. Coeur*, 69,299,1978
- [6] D. Cohen, *IEEE Trans. Mag.*, MAG-11, 694,1975
- [7] D. Cohen, *Science*, 180,745,1973
- [8] P.-L. Kalliomäki, P.J. Karp, T.E. Katila, P. Mäkipää, P. Saar, and A. Tossavainen, *Scand. J. Work. Environ. and Health*, 4,232,1976
- [9] J.R. Hughes, J. Cohen, C.I. Mayman, M.L. Scholl, and D.E. Hendrix, *J. Neurol.*, 594,1,1977
- [10] J.R. Hughes, D.E. Hendrix, J. Cohen, F.H. Duffy, C.I. Mayman, M.L. Scholl, and B.N. Cuffin, *Electroenceph. Clin. Neurophysiol.*, 40,59,1976
- [11] M. Reite, J.E. Zimmerman, J. Edrich, and J. Zimmerman, *Electroenceph. Clin. Neurophysiol.*, 40,59,1976
- [12] D. Brenner, J. Lipton, L. Kaufman, and S.J. Williamson, *Science* 199, 81,1978
- [13] S.J. Williamson, D. Brenner, and L. Kaufman, in *Future Trends in Superconductive Electronics*, B.S. Deaver, C.M. Falco, J.H. Harris, and S.A. Wolf, Eds., American Institute of Physics, New York, 1978
- [14] M. Saarinen, P.J. Karp, T.E. Katila, and P. Siltanen, *Cardiovascular Res.* 8,820,1974
- [15] J.W. Harris, D.E. Farrell, M.J. Messer, J. Tripp, G.M. Brittenham, E.H. Danish, and W.A. Muir, *Clinical Res.*, 26,3,1978
- [16] S.J. Williamson, L. Kaufman, and D. Brenner, *Biomagnetism*, in *Superconductor Applications: SQUIDS and Machines*, B.B. Schwartz and S. Foner,

- [17] B.J. Roth and J.P. Wikswo, *Biophys. j.*, 48,93, 1985
- [18] F.L. Gielen, B.J. Roth, and J.P. Wikswo, Jr., *IEEE Trans. Biomedical Engr.*, BME-33, 910, 1986
- [19] J.P. Wikswo, Jr., *IEEE Trans. Biomedical Engr.*, BME-30, 215, 1983 Eds., Plenum, New York, 1977 New York9 1983
- [20] K.S. Cole, *Membranes, Ions and Impulses*, University of California Press, Berkeley, 1972
- [21] M.B. Ketchen, T. Kopley, and H. Ling, *Appl. Phys. Lett.*, 44,1008, 1984
- [22] J. Clarke, in *Superconducting Quantum Interference Devices and their Applications*, H.D. Hahlbohm and H. Lubbig, Eds., Walter. de Gruyter, Berlin, 1977
- [23] A.H. Silver and J.E. Zimmerman, *Phys. Rev.*, 157, 317,1967
- [24] A.H. Silver and J.E. Zimmerman, in *Applied Superconductivity*, V.L. Newhouse, Ed., Academic Press, New York, 1975
- [25] J. Clarke, *Advances in Superconductivity*, NATO Advanced Science Institute, Plenum, New York, 1983
- [26] J.E. Zimmerman and A.H. Silver, *Phys. Rev.*, 141,367,1966
- [27] J. Clarke and J.L. Paterson, *Appl. Phys. Lett.*, 19,469,1971
- [28] W.C. Stewart, *Appl. Phys. Lett.*, 12,277,1968
- [29] D.E. McCumber, *J. Appl. Phys.*, 39, 3113, 1968
- [30] M.B. Ketchen, in *SQUID '80*, H. -D. H. Hahlbohm and H. Lubbig, Eds., Walter de Gruyter, Berlin, 1980
- [31] J.P. Wikswo, Jr., in *Advances in Cryogenic Engineering*, vol 33. R.W. Fast, Ed., Plenum, 1988
- [32] J.P. Wikswo, R.N. Friedman, A.W. Kilroy, J.M. van Egeraat, and D.S. Buchanan, *Proc. 7th. Int. Conf. on Biomagnetism*, Plenum, New York. (in press)
- [33] B.M. Oliver, *Proc.IRE*,49,1960,1961
- [34] A. Yariv, *Optical Electronics*, 3rd. Edition, Holt, Rinehart and Winston, New York, 1985.
- [35] R.H. Dicke, *Rev. Sci. Instrum.*,17,268,1946
- [36] H.P. Yuen and V.W.S. Chan, *Opt. Lett.*,8,177-179,1983.

- [37] J.H. Shapiro, IEEE J. Quant. Electron. QE-21, 237, 1985
- [38] A. Watanabe, Jap. J. Physiol. 36,625,1986; J. Physiol. 389,223,1987, and references therein
- [39] D.L. Mazzoni, and C.C. Davis, " Trace Detection of the Hydrazines by Optical Homodyne Interferometry," Applied Optics, 30, 756-764, 1991.
- [40] D.L. Mazzoni, K.Cho, and C.C. Davis, "A Hybrid Fiber-Optic Sensor Using True Heterodyne Measurement Techniques," Opt. Lett. 16, 614-616, 1991.
- [41] Kyuman Cho, David L. Mazzoni, and Christopher C. Davis "Measurement of the Local Slope of a Surface using Heterodyne Interferometry: A New Method in Scanning Microscopy," to be published in Optics Letters.
- [42] David L. Mazzoni, Kyuman Cho, and Christopher C. Davis, "A Coherent Hybrid Fiber-Optic Probe for Mapping Induced Birefringence in GaAs Structures," to be published in the Journal of Lightwave Technology.

## APPENDICES

1. Progress Report from Professor John P. Wikswo of Vanderbilt University, sub-contractor on this contract. "Development of NanoSQUID."
2. T.A. Bowmaster, C.C. Davis, and V. Krauthamer, "Excitation and Detection of Action Potential Induced Fluorescence Changes through a Single Monomode Optical Fiber," *Biochimica et Biophysica Acta*, 1091, 9-14, 1991
3. V. Krauthamer, H.J. Bryant, C.C. Davis, and T.W. Athey, "Action Potential Induced Fluorescence Changes Resolved with an Optical Fiber Carrying Excitation Light," *J. Fluorescence* (in press.)
4. D.L. Mazzoni, K.Cho, and C.C. Davis, "A Hybrid Fiber-Optic Sensor Using True Heterodyne Measurement Techniques," *Opt. Lett.* 16, 614-616, 1991.
5. Kyuman Cho, David L. Mazzoni, and Christopher C. Davis "Measurement of the Local Slope of a Surface using Heterodyne Interferometry: A New Method in Scanning Microscopy," to be published in *Optics Letters*.
6. David L. Mazzoni, Kyuman Cho, and Christopher C. Davis, "A Coherent Hybrid Fiber-Optic Probe for Mapping Induced Birefringence in GaAs Structures," to be published in the *Journal of Lightwave Technology*.

**PROGRESS REPORT**  
**DEVELOPMENT OF NanoSQUID**

**DAMS1790Z0052**

**John P. Wikswo, Jr., P.I.**  
**Department of Physics and Astronomy**  
**Vanderbilt University**  
**Nashville, TN**

**October 1992**

Work on this project has been directed towards several fronts. The fabrication of the high resolution nanoSQUID chip by IBM was delayed due to process problems. These problems have been corrected, and I am told by Dr. Mark Ketchen that the chips have now been fabricated with both one-half micron and one micron linewidth, but have yet to be diced and tested. When my collaborator, Dr. Claudia Tesche, returns from her sabbatical leave in Finland, we will prepare this chips and mount them in our cryostat. We have designed a cryogenic dip probe to allow us to test these in our liquid helium storage dewar, and this probe is presently being fabricated in the Physics Department Machine Shop. We have continued with our design efforts for the mounting of the nanoSQUID cryostat within the magnetic shield, and expect to conduct cryogenic tests within the next six weeks.

While awaiting the completion of nanoSQUID, we have furthered our high-resolution magnetic studies on cardiac tissue. As indicated in the enclosed conference paper, which was presented just this past August, we have obtained the first images of octupolar current patterns in cardiac tissue. As can be seen from the figure in that paper, the measurements of the magnetic field pattern for both the stimulus artifacts and the propagating wavefront are consistent with the theoretical predictions from the bidomain model. We are presently conducting model calculations to ascertain the distribution of spatial frequencies in the magnetic field map. We

believe that it is the high spatial frequencies, on the order of  $1 \text{ mm}^{-1}$  and above, for which the data can be used to discriminate between a doubly-anisotropic bidomain model and an anisotropic monodomain model. The present MicroSQUID magnetometer, with its 3 mm coils 1.5 mm from room temperature, has very limited sensitivity at the needed high spatial frequency ranges, and hence it is crucial for these studies to utilize nanoSQUID, which should definitely be able to record signals greater than  $\text{mm}^{-1}$  at the requisite spatial frequencies.

We have begun a mathematical analysis of the sensitivities and spatial resolution of SQUID microscopes such as nanoSQUID. In our study, we have assumed that the spacing between the SQUID and the sample is equal to the diameter of the pickup coil. In systems with high temperature samples and low temperature magnetometers, it is clearly necessary to utilize vacuum for thermal insulation, which in turn requires a thin vacuum window; the thickness of the window and the vacuum space are of course minimized. Optimization of the pickup coil for maximum field sensitivity and resolution indicates that the pickup coil diameter should be approximately the same as the coil-to-sample spacing set by the window and vacuum thickness. In fully cryogenic SQUID microscopes, it may be possible to get the coil to sample distance smaller than the minimum SQUID size, but this has not yet been achieved, and is not helpful for biological systems. Hence, as a first order of approximation, we have assumed that the coil-to-sample spacing is equal to the length of the side of a square pickup coil. Furthermore, we will assume that, for practical SQUID magnetometer designs, the geometry of the two Josephson junctions and the coupling washer are fixed, and that the matching of the pickup coil inductance to the SQUID inductance is done through picking the number of turns in the SQUID coupling coil deposited above the washer. In this case, the magnetometer optimization can assume a fixed value for the SQUID flux sensitivity, which we will assume to be  $10^{-6} \phi_0/\text{Hz}^{1/2}$ . The sensitivity of commercially-available SQUIDs is as much as an order of magnitude worse than this, but the

SQUIDS currently being fabricated at IBM may be at least a factor of 2 lower noise than this figure. Given a fixed flux noise, and unity coupling between the SQUID sensor and the pickup coils, the sensitivity of the magnetometer in terms of fields is simply the flux noise divided by the area of the pickup coil, implying that if our magnetometer size is reduced by a factor of 2, the field sensitivity of the magnetometer is reduced by a factor of 4. Thus the smaller the magnetometer, the lower its absolute field sensitivity. However, because smaller magnetometers can be placed closer to the sample, there should be an increase in the field produced by the source. If the source is a wire, the magnetic field strength is proportional to  $1/r$ . The sensitivity of the magnetometer can then be expressed in terms of the minimal current that can be detected in a wire, which is obtained directly from Ampere's law

$$B_{\text{wire}} = \frac{\mu_0 I}{2\pi r} \quad \text{or} \quad I_{\text{min}} = \frac{2\pi r B_{\text{noise}}}{\mu_0} = \frac{2\pi \phi_{\text{noise}}}{\mu_0 r}$$

Hence as the magnetometer is made smaller, the field strength increases as  $1/r$  and the sensitivity decreases as  $1/r^2$ , so that the minimum current detectable by the magnetometer is proportional to  $1/r$ .

The situation is somewhat better if the magnetic field source is a current dipole immersed in a conducting medium. In this case, the magnetic field is proportional to  $1/r^2$ , so that the signal-to-noise ratio, or the minimal detectable current dipole moment, is independent of magnetometer size. If the sole object of an experiment is to detect the presence of such a dipole, little is to be gained by miniaturizing the magnetometer, and in fact design compromises during the miniaturization process may in fact lead to reduced sensitivity. On the other hand, if the object of the experiment is to locate the wire or image a distribution of current dipoles, it is clearly advantageous to use miniature magnetometers because of their increased spatial resolution. We are presently attempting to devise a figure of merit that allows us to quantify

the combined measures of both detectability and spatial resolution to aid in our optimization of SQUID microscopes.

The advantages of magnetometer miniaturization are more obvious for magnetic fields that are produced by magnetic dipoles. Since the magnetic field scales as  $1/r^3$  while the sensitivity scales as  $r^2$ , the magnetic dipole detectability goes as  $1/r$ . This is why the relatively insensitive magnetometer used in a magnetic tape recorder can give very large signals: the spacing between the magnetic dipoles and the tape head can be on the order of a micron or less. Similarly, the magnetic force microscope is an intrinsically insensitive magnetometer, but for imaging the strong magnetic dipoles written on a computer disk, it can obtain a spatial resolution on the order of 10 nanometers with tip to surface spacings of a nanometer. Unfortunately, the field sensitivity of this type of device is five orders of magnitude worse than what can be achieved with a SQUID microscope.

Based on this analysis, we recognize that the optimization of a SQUID microscope is governed not only by the nature of the source, but also by the intended measurement. In all cases, the performance of the instrument is determined directly by the sensitivity of the SQUID, and, in this context, it is most reassuring that the new thin film, integrated SQUIDs being produced by IBM have an order of magnitude lower noise than presently-available commercial dc SQUIDs. As we continue to develop the cryogenic systems needed to exploit the sensitivity of these SQUIDs for biological measurements, we anticipate a steady increase in the performance of high resolution SQUID magnetometers over that already achieved with MicroSQUID. The simultaneous development of improved instrumentation, more detailed mathematical models, and suitable tissue preparations and measurement techniques should enable us to make significant contributions to a broad range of biophysical problems.

# Excitation and detection of action potential-induced fluorescence changes through a single monomode optical fiber

Thomas A. Bowmaster<sup>1</sup>, Christopher C. Davis<sup>1</sup> and Victor Krauthamer<sup>2</sup>

<sup>1</sup> *Electrical Engineering Department, University of Maryland, College Park, MD (U.S.A.) and*

<sup>2</sup> *Division of Physical Sciences, Food and Drug Administration, Center for Devices and Radiological Health, Rockville, MD (U.S.A.)*

(Received 16 July 1990)

**Key words:** Optical recording; Optical fiber; Action potential; Voltage-sensitive dye; Membrane fluorescence; Frog heart

An optical probe capable of detecting intracellular potential changes in individual cells, *in vitro*, which has the potential for *in vivo* applications, has been developed. A single-mode optical fiber directs laser light onto cells stained with the voltage-sensitive fluorescent dye, WW781 and also returns part of the resulting fluorescence to a detection system. Frog cardiac cells *in vitro* were used in these initial experiments. The fractional change in fluorescent intensity of  $10^{-3}$  for a 50 mV shift in transmembrane potential obtained from a heart immobilized in zero calcium Ringer's solution is comparable to that reported for other optical methods. For hearts in normal calcium Ringer's solutions, very large reproducible motion related artifacts were detected.

## Introduction

For many years the electrical activity of cells in various organisms has been of interest to researchers. During this time, two of the primary methods for detecting and measuring electrical activity have been extracellular electrodes that measure potential differences between different areas of the sample and intracellular microelectrodes that penetrate the cell and measure the potential across the cell membrane. Recently, optical methods have been developed that offer more direct information than extracellular recording and do not require penetration of the cell. In these methods a sample is stained with a voltage-sensitive dye whose fluorescence, absorption, or in some cases birefringence changes linearly in response to changes in the membrane potential of a cell [1,2]. Over 1800 dyes have been tested for appropriate optical responses and for toxic effects on various specimens [3]. Of these, approx. 200 have been shown to exhibit significant optical changes without causing excessive pharmacological side effects or photodynamic damage. Many of these dyes are classified as fast response dyes and respond on a microsecond time scale to membrane potential changes. The fractional change in fluorescence or absorption for these dyes is on the order of  $10^{-3}$  to  $10^{-4}$  per 100 mV and a

variety of mechanisms have been proposed to explain their spectra and optical responses [4]. The relative change in fluorescence intensity from these dyes has been shown to be a linear function of the change in transmembrane voltage [1,2,5]. For absolute calibration of the fluorescence/voltage response the dye must be calibrated against an electrical recording made in the same cellular material.

A number of the fast response dyes have been used to detect or map action potential propagation in various preparations. The earliest studies were in squid axon [1,6,7] and invertebrate central neurons [8,9]. More recent studies have examined excitation spread in heart [10,11], remote regions of cultured neuroblastoma cells [12], intact whole salamander brain [13], nerve terminals of the amphibian neurohypophysis [14] and dendrites in the barnacle central nervous system [15,16]. In most of these studies the stained samples were placed on the stage of a microscope and illuminated over a relatively large area. A photodiode array placed in the objective image plane was then used to detect the optical signal of interest. Usually the source of illumination has been a tungsten-halogen or mercury arc lamp with various filters used to select an appropriate wavelength [1-3]. In a variation of this method, a Helium-Neon laser has been used to scan across a stained preparation, allowing a single detector to record from multiple sites [10-12].

While the methods used so far have worked quite well for *in vitro* studies, they have severe limitations for *in vivo* measurements. In those cases where absorption

Correspondence: C.C. Davis, Electrical Engineering Department, University of Maryland, College Park, Maryland 20742, U.S.A.

changes are measured directly, some components of the detection system must be located behind the sample, opposite the illumination source. For many in vivo systems of interest this configuration is impractical. For fluorescence measurements and cases where the absorption is measured by the changes in the the backscattered excitation light, the excitation and detection systems can be located on the same side of the sample, but a line of sight path between these systems and the preparation is required [17]. Use of optical fibers to direct the excitation and fluorescence light would allow measurements to be made in organisms where a direct optical path is not available [18,19]. By using one single-mode fiber to carry both the excitation light and the fluorescence, the diameter of the area studied can be limited to approx.  $4\text{ }\mu\text{m}$ , (the core diameter of the fiber). This high spatial resolution is a fundamental geometric property of a single-mode fiber, which can only illuminate a small area of a cell membrane that is directly under it. Such a fiber allows greater spatial resolution than the photodiode arrays used previously, which typically measured from areas on the order of  $40 \times 40$  to  $100 \times 100\text{ }\mu\text{m}^2$  [10,16,20]. If separate single-mode fibers (with typical cladding diameters of  $125\text{ }\mu\text{m}$ ) were to be used to carry the excitation light and the fluorescence they would have to be relatively far from the surface for both of them to be directed at the same spot. This would cause a much larger area to be illuminated, and would also reduce the collection efficiency [21]. High collection efficiency can be maintained, with a concomitant similar reduction in spatial resolution by the use of pairs of multimode optical fibers [18,21]. A single multimode fiber could also be used, but its large core diameter intrinsically prevents the attainment of high spatial

resolution. The use of a single monomode fiber promises the highest theoretical spatial resolution, yet with some additional experimental difficulty. These fibers are less forgiving of misalignment than multimode fibers and lower fluorescence throughput is inevitable.

One drawback of the use of a single optical fiber is that absorption changes can not be measured. Absorption measurements would have to be made using backscattered light from the sample. This backscattered light would take the same optical path and have the same wavelength as the excitation light reflected at the ends of the fiber, so it would not be possible to separate them. The reflected light would add considerable noise to the signal. In fluorescence measurements an optical filter can be used to separate the longer wavelength fluorescence from the reflected excitation light. Another drawback is that the use of a single-mode fiber reduces the detected light levels considerably. Calculations of the fluorescence intensity returned by the fiber to the detection system indicate that a photomultiplier tube would be optimal rather than a photodiode detector, and that shot noise is the limiting noise factor [22].

## Materials and Methods

### *Voltage-sensitive dye*

The dye WW781 (Molecular Probes, Eugene, OR) was chosen for these initial experiments for a number of reasons. In particular, it can be excited using a Helium-Neon laser and has previously been used successfully in a variety of preparations [10-12,25]. Its other beneficial features include its low toxicity and the minimal photodynamic damage that it causes [4,23]. As with all voltage-sensitive dyes, however, it is subject to bleaching

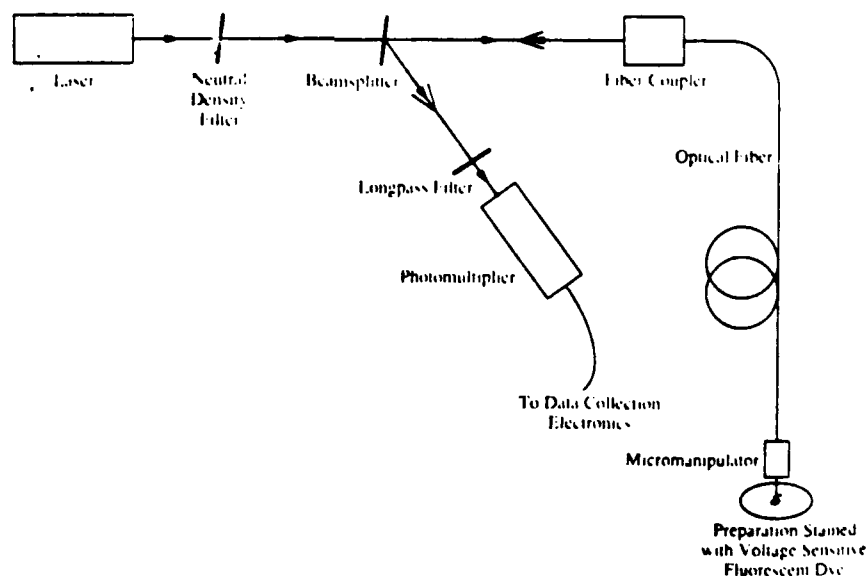


Fig. 1. Optical apparatus. Excitation light at 633 nm is emitted from a He-Ne laser, attenuated by a neutral density filter and passed into a single-mode optical fiber with a  $4\text{ }\mu\text{m}$  diameter core. Fluorescence from the tissue (represented by double arrows) travels back through the fiber and wavelengths greater than 650 nm are reflected by the beamsplitter into the photomultiplier. See text for further details.

when exposed to intense illumination. For the experiments conducted here, it was decided to use the highest incident intensity that did not cause extensive bleaching, as evidenced by a minimal fluorescence baseline drift, and then use signal averaging to increase the signal-to-noise ratio.

#### *Optical setup*

The optical setup is shown in Fig. 1. The laser used was a 10 mW Helium-Neon laser (model 105-1, Spectra-Physics, Eugene, OR). The output of this laser exhibited some amplitude modulation at 120 Hz and 25 kHz (the switching frequency of the laser power supply). In these experiments shot noise was the limiting noise factor. We were looking for signals with very low frequency components so the effects of the laser amplitude modulation were removed by passing the detected signals through a lowpass filter. Alternatively, we have available a laser amplitude stabilization unit (EOD Stabilaser, Tecoptics, Merrick, NY) that reduces amplitude noise by 50 dB from 0–10 kHz, but its use was not required in the experiments described here. The laser output also varied in a random manner because of feedback reflections from the fiber coupler. This noise was significantly reduced when a neutral density filter was inserted into the beam path. By placing the filter at a slight angle to the beam almost all reflections back into the laser cavity were eliminated.

A 100× neutral density filter (model NG9, Schott Glass Technologies, Duryea, PA) was used in most of the experiments. In addition to reducing the feedback to the laser, this filter also slowed the dye bleaching, allowing the fluorescence baseline drift to be neglected. The beamsplitter was a shortpass interference filter (model SP675, Oriel Corp., Stratford, CT) placed so that its normal was at an angle of 34 degrees to the beam. At that angle the filter passed approx. 80 of the laser light but reflected 95% of the returning fluorescence.

After passing through the beamsplitter, a fiber coupler (model F-1015, Newport Research Corp., Fountain Valley, CA) was used to focus the laser light onto the end of an optical fiber. The fiber coupler contained a 20×, 0.40 numerical aperture microscope objective. The optical fiber used was Newport F-SV, which is single-mode fiber with a core diameter of 4 μm. The fiber was positioned in the tissue with a micromanipulator.

Fluorescence and reflected laser light travelled back through the fiber and fiber coupler to the beamsplitter. To remove any reflected laser light a Schott RG665 longpass colored glass filter was placed in front of the detector. A photomultiplier (model 56TVP, Philips, through Amperex Electronic Corp., Hicksville, NY) was used to detect the fluorescence.

#### *Signal processing*

The current output of the photomultiplier tube was converted to a voltage signal through a 10 kΩ resistor. This voltage was amplified and displayed on an oscilloscope. The signal was typically a 0.1% fluorescence change over baseline. It was necessary to filter the D.C. component of the signal before it was digitized by a waveform recorder with 10 bit accuracy (model 5180A Hewlett-Packard, Santa Clara, CA). A 10 s time constant RC filter was used for this high-pass function along with a pair of 1.4 ms time constant low-pass filters.

#### *Electrophysiological equipment and procedures*

For all of these experiments the cells that were examined were leopard frog (*Rana pipiens*) heart muscle cells. Our choice of these cells was not spurred by a desire to apply optical recording methods involving optical fibers to intact hearts [24], but was rather motivated by the fact that these cells are known to give good optical signals and are convenient to use in test experiments. The frogs (Wards Natural Science, Rochester, NY) were maintained at 10°C. The heart was opened from the right atrium to the apex and pinned, endocardial surface up, onto a paraffin dish where it was bathed with either normal or zero Ca<sup>2+</sup> Ringer's solution. The composition of the zero Ca<sup>2+</sup> Ringer's solution was; 116 mM NaCl, 2 mM NaHCO<sub>3</sub>, and 3 mM KCl. For the normal Ringer's solution 1 mM CaCl<sub>2</sub> was added [25]. The heart was covered for 30 to 60 min with a dye solution containing 0.1 mg of WW781 per ml of Ringer's solution and was rinsed with the appropriate Ringer's solution. Hearts used in zero Ca<sup>2+</sup> had to sit for at least an additional 3 h before motion in the heart was completely suppressed.

Direct electrical recordings were made from the heart for the dual purpose of forming a basis of comparison with the optical recordings and as a means of synchronizing signal averaging. Extracellular electrodes consisted of two 36 gauge copper wires positioned approx. 1 cm apart in the ventricle and connected to an A.C. preamplifier (model P15, Grass Medical Instruments, Quincy, MA) to give an EKG signal. In some experiments an intracellular glass microelectrode was also placed in the heart and connected to a microelectrode amplifier (model 8100-1, Dagan Corp., Minneapolis, MN). When necessary, stimulation pulses of 200 μs duration, delivered via platinum electrodes, were used to pace the heart.

#### **Results**

##### *Detection of action potentials*

Fig. 2 shows examples of recorded waveforms in which the optical signals indicate the occurrence of an action potential. These waveforms were recorded from a

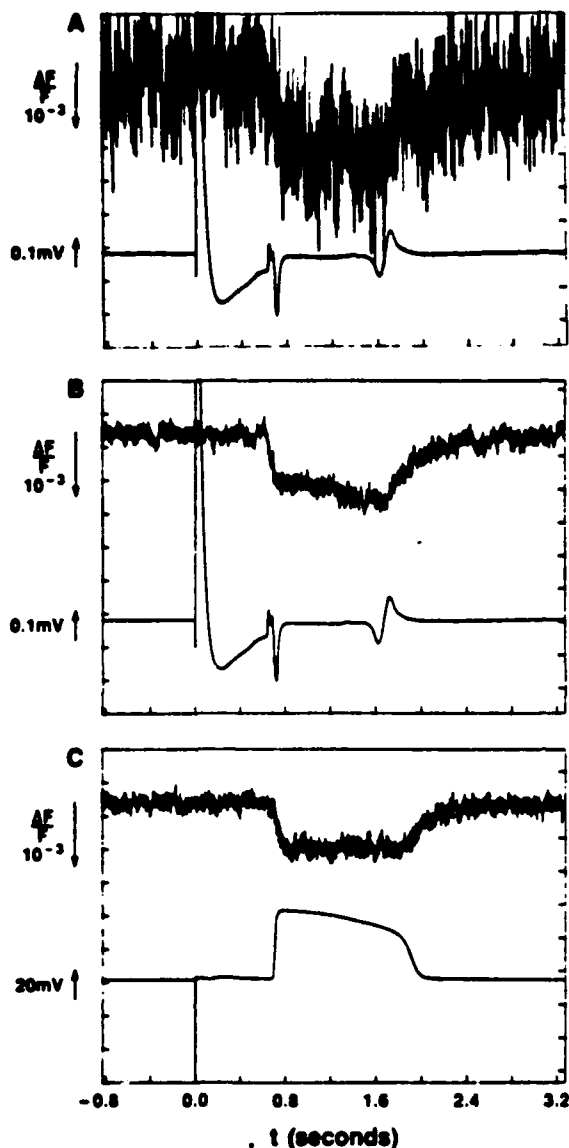


Fig. 2. Cardiac action potential signals. (A) Simultaneous optical (upper traces) and EKG (lower traces) recordings of cardiac action potentials. Heart was bathed in  $0 \text{ Ca}^{2+}$  Ringer's solution for over 4 h to suppress all movement. A stimulating pulse was required to evoke the action potentials. Single sweep. (B) Same as in (A). Average of 30 Sweeps. (C) Simultaneous optical and intracellular electrode recordings of cardiac action potentials. The resting potential was  $-50 \text{ mV}$ . Same heart as in (A) and (B). Average of 30 sweeps.

heart whose movement had been completely suppressed with zero  $\text{Ca}^{2+}$  Ringer's solution. This heart was not spontaneously active and therefore had to be paced.

Fig. 2a is a single event and Figs. 2b and 2c are the averages of 30 individual records. In all three figures the top trace is the optical signal and the bottom trace is the simultaneous electrical recording. The vertical scales for these and other similar figures are indicated by the arrows to the left of the plots. For the optical signals the arrows point in the direction of an increase in fluorescence and the length of an arrow corresponds to the

value of  $\Delta F/F$  printed next to it. For the electrical signals the arrows point in the direction of positive voltage and the length of an arrow corresponds to the value of  $\Delta V$  printed next to it.

In Figs. 2a and 2b the electrical recordings were obtained from the extracellular electrodes. The largest event on the electrical trace occurs at 0 seconds and is the stimulus artifact. The next deflection, beginning at 650 ms, is the QRS wave which indicates the start of action potentials at the electrodes. The slower deflection at about 1600 ms is the T wave and indicates the end of the action potential.

The shape of the electrical recordings from extracellular electrodes depends on the physical separation between the electrodes and the fact that the action potentials occur at slightly different times in different areas of the heart. For this reason the electrical signals shown in Figs. 2a and 2b only show the approximate timing of the action potentials at the spots being measured by the optical probe. A more accurate comparison of the timing between electrical and optical signals was obtained using an intracellular microelectrode. Since the microelectrode is extremely small it can be inserted very close to the end of the optical fiber. Fig. 2c shows the result when this was done. In this figure the stimulation pulse appears at  $t = 0$ , and the action potential lasts from 700 ms to about 2000 ms. The electrical filtering used to obtain Fig. 2c was identical for both optical and electrical recordings. Also in this figure it can be seen that the rise time of the optical signal is slightly longer than that of the electrical signal. This result was also observed in most of the other recorded waveforms: it was not caused by electrical filtering, but could be due to the limited spatial resolution of the fiber in the  $z$  direction, since the timing of the action potentials at different depths may vary [10]. This does not invalidate our previous statements about the potential high spatial resolution of the single monomode probe. In this case the test tissue masks this resolution because cells at different depths below the fiber tip are being illuminated. In other preparations this need not occur.

#### Movement related signals

The movement related signals (Fig. 3) that were recorded using the fiber optic probe were several orders of magnitude larger than those reported previously by other researchers using different detection schemes [25]. The dye was necessary for these signals to appear, as movement related signals were not detected from unstained preparations. In most cases other researchers have reported motion signals that were slightly larger than the electrically generated optical signals, or changes of  $\Delta F/F$  from about  $10^{-2}$  to  $10^{-3}$ . In these experiments, values of  $\Delta F/F$  of 5 were occasionally seen and values of 0.5 were regularly detected. These movement related signals may have some diagnostic value in their

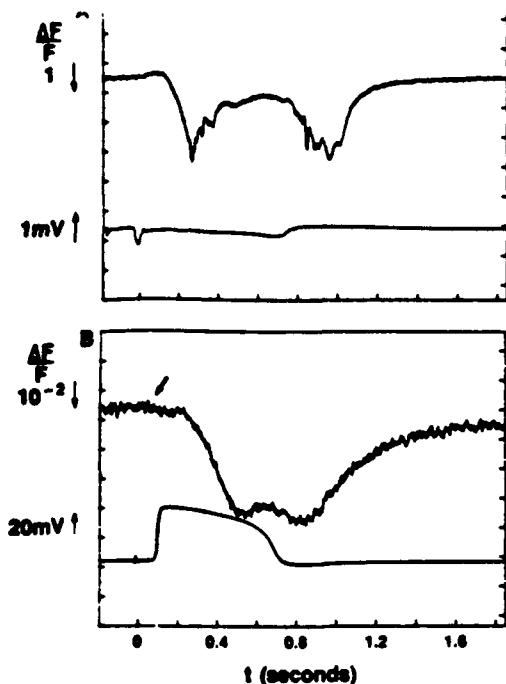


Fig. 3. Movement-related signal. (A) Simultaneous optical and EKG recordings from a heart in normal  $\text{Ca}^{2+}$  Ringer's solution. Note the magnitude of the fluorescence change is over 200%. Optical recording shows two peaks which apparently correspond to contraction of the heart and relaxation back to the resting position. Average of 10 sweeps. (B) Simultaneous optical and intracellular electrode recordings from a heart in very low  $\text{Ca}^{2+}$  Ringer's solution. Stimulation pulse was required. Action potential is visible in optical signal at 0.1 s (indicated by arrow). Much larger movement related signal occurs almost 200 ms after the start of the action potential. Average of 25 sweeps.

own right, independent of optical recording of changes in trans-membrane potential.

Fig. 3a is an example of this type of signal. The amplitude of the large movement signals was practically constant when the  $100\times$  neutral density filter was used, but decayed fairly quickly in early experiments using a  $10\times$  neutral density filter. The decay in the amplitude of the signals is due to bleaching, rather than a decline in the signals themselves.

Although a majority of the movement signals were in the direction of increased fluorescence, occasionally a signal was obtained where there was a decrease in fluorescence. This type of signal could be obtained by positioning the end of the fiber near the edge of a darkly stained area so that contraction caused a lightly stained area to move into the illuminated region. Also, in some cases where the heart was beating vigorously it was difficult to determine the polarity of the signal since there didn't appear to be a resting baseline.

There are two explanations for the findings that the movement-related signals are larger than those previously reported and consistently in the direction of increased fluorescence (with the noted exception above).

The first explanation is that the muscle contraction moves the surface closer to the fiber causing a large increase in the amount of fluorescence collected. The second is that lateral displacement of the muscle brings 'fresh' (unbleached) dye into the narrow field-of-view of the fiber causing a temporary increase in the amount of fluorescence. In other systems, which collect the light with a lens, the preparations are diffusely illuminated, so that bleaching is isotropic and light collection does not vary much with small changes in distance.

All movement was suppressed in the heart from which the records shown in Fig. 2 were obtained. In addition to not being able to see any movement when the heart was viewed through the microscope, two other indicators support this statement. The first of these was that the speckle pattern around the end of the fiber was stationary. It did not flicker at all after a stimulation pulse. The other indicator was the simultaneity of the electrical and optical signals [20]. As Salama [25] has discussed, there is a delay of approx. 200 ms between an action potential and the contraction that it causes. This delay is apparent in Fig. 3b for a heart which exhibited a very small amount of movement. This figure was obtained by adding two drops of normal  $\text{Ca}^{2+}$  Ringer's solution to the dish containing the heart used in the earlier experiments. After several minutes, the speckle pattern at the end of the fiber began to flicker after each stimulus and a tiny amount of movement could be seen through the microscope.

## Conclusions

These experiments demonstrate that action potentials in frog cardiac cells can be detected with a single optical monomode fiber probe. This represents a potential improvement over the previously used optical techniques in that it may allow recordings to be made from intact animals. Also, the improved spatial resolution available with single-mode fiber may allow recordings to be made from the fine processes of cells that previously could not be examined.

The primary drawbacks of the optical fiber probe are the large movement related signals and the low detected light levels that made it necessary to use signal averaging to obtain an adequate signal-to-noise ratio. Several possible improvements to the system used in these experiments would increase the detected light levels and therefore reduce the effect of shot noise on the signals. These include the use of a photomultiplier with better sensitivity at the fluorescence wavelengths, and the use of a fiber with a larger core diameter. A larger diameter core would increase the collection efficiency of the fiber, but would also decrease the available spatial resolution. Another way to increase the light levels would be to increase the incident intensity by replacing the neutral density filter with one that is more trans-

compensate for the fluorescence baseline drift that would result from bleaching of the dye and it would not be possible to signal average as long. Grinvald et al. [26] have described one way that the baseline drift compensation can be accomplished.

Although in these experiments the cardiac action potentials were recorded from only one spot at a time, there is no reason the system could not be expanded to include several fibers simultaneously recording from different areas in the sample. This could allow the propagation of the action potentials to also be examined. To do this a single laser could be used and with the use of fiber couplers illuminate several fibers. A separate optical detection arrangement would be needed for each returning fluorescence signal, although in principle this could involve a fiber bundle and an optical detector array. The simplest multiplexing we envisage would involve the use of two separate probes for mapping the transit of electrical signals in tissue, or between cells.

Future research will determine if the use of an optical fiber probe can be successfully extended to measure electrical activity in preparations other than frog heart, possibly leading to in vivo use in situations where a direct line of sight path is not available.

#### Acknowledgements

This research was partially supported by the Food and Drug Administration through contract FDA-503918-01-87/R. We wish to thank Dr. Brian Salzberg for suggesting the use of frog heart in these initial experiments and Ms. Catherine Ruseau for doing some of the initial work in setting up the apparatus.

#### References

- 1 Cohen, L., Salzberg, B., Davila, H., Ross, W., Landowne, D., Waggoner, A. and Wang, C. (1974) *J. Membr. Biol.* 19, 1-36.

- Membr. Biol.*, 58, 123-137.
- 3 Grinvald, A. (1985) *Annu. Rev. Neurosci.* 8, 263-305.
- 4 Waggoner, A. (1979) *Annu. Rev. Biophys. Bioeng.* 8, 47-68.
- 5 Cohen, L.B. and Salzberg, B.M. (1978) *Rev. Physiol. Biochem. Pharmacol.* 85, 35-88.
- 6 Davila, H.V., Salzberg, B.M., Cohen, L.B. and Waggoner, A.S. (1973) *Nature New Biol.* 241, 159-160.
- 7 Tasaku, I., Watanabe, A., Sandlin, R. and Carnay, L. (1968) *Proc. Natl. Acad. Sci. USA* 61, 883-888.
- 8 Salzberg, B.M., Davila, H.V. and Cohen, L.B. (1973) *Nature*, 246, 508-509.
- 9 Salzberg, B.M., Grinvald, A., Cohen, L.B. and Ross, W.N. (1977) *J. Neurophysiol.* 40, 1281-1291.
- 10 Hill, B. and Courtney, K. (1987) *Annu. Biomed. Eng.* 15, 567-577.
- 11 Dillon, S. and Morad, M. (1981) *Science* 214, 453-455.
- 12 Grinvald, A., Ross, W. and Farber, J. (1981) *Proc. Natl. Acad. Sci. USA*, 78, 3245-3249.
- 13 Kauer, J. (1988) *Nature* 331, 166-168.
- 14 Salzberg, B., Obaid, A., Senseman, D. and Gainer, H. (1983) *Nature* 306, 36-39.
- 15 Krauthamer, V. and Ross, W. (1984) *J. Neurosci.* 4, 673-682.
- 16 Ross, W. and Krauthamer, V. (1984) *J. Neurosci.* 4, 659-672.
- 17 Orbach, S. and Cohen, L. (1983) *J. Neurosci.* 3, 2251-2262.
- 18 Dillon, S. and Wit, A. (1988) *Biophys. J.* 53, 641a.
- 19 Kudo, Y., Takeda, K., Hicks, T.P., Ogura, A. and Kawasaki, Y. (1989) *J. Neurosci. Meth.* 30, 161-168.
- 20 Hill, B. and Courtney, K. (1982) *Biophys. J.* 40, 255-257.
- 21 Snyder, A. and Love, J. (1983) in *Optical Waveguide Theory*. Chapman and Hall, London.
- 22 Bowmaster, T. (1988) Masters Thesis, University of Maryland.
- 23 Morad, M., Dillon, S. and Weiss, J. (1986) in *Optical Methods in Cell Physiology*, Chapter 12 (DeWeer, P. and Salzberg, B., eds.) Wiley Interscience, New York.
- 24 Dillon, S.M. and Wit, A.L. (1988) *Proceedings of the 10th Annual Meeting of the IEEE Engineering in Medicine and Biology Society*, 215-216.
- 25 Salama, G. (1988) in *Spectroscopic Membrane Probes* (Loew, L., ed.), CRC Press, Boca Raton.
- 26 Grinvald, A., Salzberg, B., Lev-Ram, R. and Hildesheim, R. (1987) *Biophys. J.* 51, 643-651.

**ACTION POTENTIAL INDUCED FLUORESCENCE CHANGES RESOLVED WITH AN  
OPTICAL FIBER CARRYING EXCITATION LIGHT**

Victor Krauthamer<sup>1</sup>, Howard J. Bryant<sup>2</sup>, Christopher C. Davis<sup>3</sup> and  
T. Whit Athey<sup>1</sup>

<sup>1</sup>Food and Drug Administration, Center for Devices and  
Radiological Health, Division of Physical Sciences (HFZ-133),  
Rockville, MD 20857, <sup>2</sup>Uniformed Services University of the Health  
Sciences, Department of Physiology, Bethesda, MD 20814 and  
<sup>3</sup>University of Maryland, Department of Electrical Engineering,  
College Park, MD 20742

corresponding author: Victor Krauthamer, (301)443-3840

running head: Fiber-Optic Recording from Potentiometric Dyes

**ABSTRACT**

With the use of a single, implantable, optical fiber, to excite fluorescence and detect changes from voltage-sensitive dyes, transmembrane potential changes were measured without the need for a clear line-of-sight path between the excitation light, tissue and detector. In a previous study, we were required to use signal averaging and could only detect cardiac action potentials from frog. In the present study we improved this system so that unaveraged cardiac action potentials were resolved with high fidelity, and action potentials from single nerve axons were detected. Endeavors to optimize the signal-to-noise ratio resulted in the selection of: a larger core fiber with a rounded tip, styryl dyes, and filters based upon fluorescence spectra of the dyes when bound to membrane (rather than in solution). The frog gave signals nearly comparable in magnitude and signal-to-noise ratio to those seen with systems that use a fluorescence microscope. Action potential-induced signals could be detected in single lobster axons with the intracellular injection of a dye. The improvement in signal-to-noise ratio allowed the use of a reduced intensity excitation illumination which produced less bleaching of the dye.

**Key words:** Voltage-sensitive Dye, Optical fiber, Fluorescence,  
Lobster axon, Frog heart, Laser

## INTRODUCTION

Optical recording of electrical activity in excitable cells with voltage-sensitive dyes has been used by neurobiologists for some time [5]. Dyes exist that produce linear changes in absorption of transmitted light or fluorescence from excitation light. Two advantages of optical recording of voltages are the ability to make; 1) intracellular recordings simultaneously from many sites that could not be penetrated by microelectrodes [10, 15], and 2) recordings that are isolated from stimulus artifacts [4].

Until recently, the use of optical recording has required extensive dissection because of the necessity of a direct line-of-sight path between the living tissue and the recording system, usually utilizing a microscope. Two recent works with optical fibers have only partially obviated this constraint. Dillon [3, 4] employed a multiple fiber system in which excitation light was emitted from one fiber and the fluorescence detected by other fibers in the bundle. Kudo et al. [11] used two fibers held in a micropipette for exciting and detecting respectively, the fluorescence from a calcium-sensitive dye. As a result of the use of more than one fiber in both of these systems, spatial resolution is limited, areas directly under the excitation fiber (that receive the most fluorescence excitation) are not closest to the detection fiber, and significant tissue disruption would occur if these fiber systems were implanted. In

our previous preliminary work [1], we described a technique for using a single, implantable, fiber for both delivering the excitation light and carrying the fluorescence to a detector. The technique suffered from a poor signal-to-noise ratio that required the averaging of multiple events, and the signals could only be detected from cardiac muscle, not neurons. The capability of this system was limited by; 1) the high concentration of dye required, 2) the low intensity of the fluorescence generated by the dye and 3) the fluorescence collection capability of the 4  $\mu\text{m}$ -core fiber. The latter two limitations affect the size of the optical signal. In this paper we describe improvements to this system, which now can be used with different dyes at lower concentrations, and that permit clear resolution of single (unaveraged) cardiac action potentials and the detection of action potentials from single lobster axons.

## MATERIALS AND METHODS

### Animal Preparations:

Frogs (Rana pipiens) were obtained from Carolina Biological Supply (Burlington, NC), and their hearts were prepared as described by Bowmaster et al. [1]. The formulae for the frog saline solutions have been described by Salama [16]. To prevent

movement, the hearts were bathed in a calcium-free saline solution. Lobsters (Homarus americanus) were obtained from local fish markets, and their circumesophageal connectives were removed according to the method of Dalton [2]. The saline solution used was from Maynard and Walton [12].

#### Optical Recording Apparatus:

The arrangement for the optical recording is illustrated in Fig. 1. The light source was either a red (633 nm) helium-neon laser (Spectra-Physics, Mountain View, CA, model 105-1, 5 mW) or a green (543 nm) helium-neon laser (Siemens, Iselin, NJ, model LGK-7770, 0.5 mW) depending upon whether a red-excited oxonol dye (WW781) or a green-excited styryl dye (RH237, RH414 or RH461) was used. The laser light was attenuated by a neutral density filter (by a factor ranging from  $10^1$  to  $10^5$ ), a procedure necessary to reduce the extent of dye bleaching. The light next passed through an angled, short-pass, interference filter (Oriel, Stratford, CT, model SP675nm for red excitation, or model SP575nm for green excitation). This filter served as a dichroic beam-splitter, where the longer wavelength fluorescence was reflected to the photodetector. The light was next focused into the fiber through a X20, 0.40-numerical aperture microscope objective held in a fiber coupler (Newport, Fountain Valley, CA, model F-1015). The three fibers used (Newport models SW, MSD, and MLD) had core diameters of 4  $\mu\text{m}$ , 50  $\mu\text{m}$  and 100  $\mu\text{m}$  and

cladding diameters of 125  $\mu\text{m}$ , 125  $\mu\text{m}$  and 140  $\mu\text{m}$  respectively. For some experiments, the tip of the 100  $\mu\text{m}$  core fiber was rounded (into a hemispherical shape) by melting it with a hydrogen torch, in order to form a crude lens. The fiber end was held by a micromanipulator and placed in the stained tissue. Returning fluorescence was focused by the microscope objective and reflected by the dichroic beam-splitter (angled short-pass filter). A long-pass barrier filter (Schott, Duryea, PA, model RG665nm for red excitation or model OG570nm for green excitation) was used in front of the detector to prevent reflected laser light from reaching the detector. The fluorescence detector was usually a photomultiplier tube (Hamamatsu, Bridgewater, NJ, model R1333) operated at -1.5 kV and terminated with a 10 K $\Omega$  resistor as a current-to-voltage converter. A photodiode (Hamamatsu model S2386-44K) was employed for detection of high light intensities. Without neutral density filters, the light transmission from the laser to the end of the 100 $\mu\text{m}$  core fiber was 40%. Moreover, with the system configured for green excitation, 95% of the light (at 633 nm) that entered the fiber was detected by the photomultiplier tube.

#### Voltage Sensitive Dyes:

Initial experiments with frog heart [1] used the oxonol dye WW781 (available from Molecular Probes, Eugene, OR) as has been used in a number of previous studies (see Salama [16]). The dye

was applied at a concentration of 1 mg/ml (1.32 mM) for 30 minutes and gave a fractional change in fluorescence of 1/1000 for a cardiac action potential. We also chose to try certain styryl dyes that reportedly can be used at micromolar concentrations with fractional fluorescence changes approximately ten times greater in magnitude than oxonol dyes [6, 7].

In the frog heart the styryl dye RH237 (Molecular Probes) was used. It was dissolved in 100% ethanol to a concentration of 3.8 mM. This dye-ethanol solution was diluted 1/100 with saline solution to obtain a final concentration of 38  $\mu$ M (20  $\mu$ g/ml) and applied to excised frog heart or lobster nerve for 30 minutes.

In the lobster axon the only dye that produced a signal was the intracellularly-injected styryl dye RH461. The technique of Grinvald et al. [7] was followed, in which microelectrodes were filled with a 100 mM solution of the dye in distilled water and positive current was used to iontophorese the dye into the cells. None of the extracellular dyes tried, including WW781, RH237 and RH414 (1 mg/ml in saline [6]) produced any detectable signal.

#### Electrophysiological Recording:

Standard techniques were employed for electrophysiological stimulation and recording. The instruments used were a Grass SD9 stimulator (Quincy, MA) for stimulation, a Grass P15 preamplifier for extracellular (electrocardiographic) recording, and a Getting

5A microelectrode system (Iowa City, IA) for intracellular recording. Microelectrodes were pulled from 1.0 mm thin-walled tubing (0.75 mm, inner diameter) and had resistances of 20 M $\Omega$  when filled with 4 M potassium acetate and 70 M $\Omega$  when filled with 100 mM WW781. Extracellular stimulation of lobster nerve fibers was accomplished with a suction electrode fabricated from polyethylene tubing.

## RESULTS

### Fiber Types:

Larger multimode fibers have the advantage of better light collection efficiency. This was tested with some fluorescence measurements. Table I compares the amount of green laser light emitted from various core diameter fibers with the amount of fluorescence returned from a dye (1 mg/ml WW781). Light intensities were measured with a photodiode and the values were normalized to those of the 4  $\mu$ m fiber. The main finding was that the 100  $\mu$ m core fiber allowed a return of 80 times as much fluorescence per unit of excitation illumination as the 4  $\mu$ m core fiber.

A second advantage of the larger multimode fibers is their greater ability to collect light at a distance. This is

illustrated by fig. 2 in which are illustrated plots of percent maximal fluorescence intensity as a function of fiber distance from a flat fluorescence source. The principal finding to emerge from these graphed relationships was that there occurred a decreased attenuation with multimode fibers (half intensity at 100  $\mu\text{m}$ ) compared with the single-mode fiber (half intensity at 25  $\mu\text{m}$ ).

#### Styryl Dyes:

The styryl dyes, as compared with the oxonol dyes, have the advantage of generating stronger signals, and of being employable at low concentrations [6, 7]. Fig. 3 illustrates fluorescence spectra from one of these dyes (RH237) in solution when bound to mouse neuroblastoma cells. The mouse cells were selected because they remain viable in suspension during the measurement of their spectra. The dye is about ten times as fluorescent when bound to cells as it is free in solution, and the fluorescence emission spectrum is shifted to the left. The peak excitation of the dye bound to cells is at 498 nm when emission is measured at 664 nm. We found that, by using 10 nm band-pass filters between 590 and 700 nm, the action-potential-related signal was broad-banded, and the long-pass filter allowed us to detect the entire signal.

#### Recordings from Heart:

The dye RH237 gave signals with a high signal-to-noise ratio when a 100  $\mu\text{m}$  core fiber was used (fig. 4a). The heart that generated the signal was spontaneously rhythmic. The upper trace is an electrocardiogram with a QRS complex at 0 msec and a T-wave at 900 msec; the lower trace is the optical signal which reflects the cardiac action potential. This optical signal is expressed as a change in fluorescence over baseline ( $\Delta F/F$ ). It was possible to average the optical signal (middle trace) because bleaching of the dye was not a significant problem at the excitation intensity used. It took approximately 40 minutes of continuous illumination for the fluorescence intensity to drop to half intensity. One interesting feature of the 100  $\mu\text{m}$  core fiber was that the movement artifact that occurs in beating hearts when calcium was present, is less than with the 4  $\mu\text{m}$  core fiber [1]. The lower trace of Fig. 4b illustrates this. The trace begins with the depolarization within 10 msec of the stimulus (time 0); it is followed after 100 msec by a second deflection which represents the contraction; the third deflection, at 570 msec, simultaneous with the T-wave, represents repolarization; relaxation occurs after 700 msec. The size of the part of the signal related to movement varied greatly and depended on the location of the fiber in the heart.

As a basis for comparison with the technique of Bowmaster et al. [1], who employed a 4  $\mu\text{m}$ -core fiber, we repeated the work employing a 100  $\mu\text{m}$ -core fiber. The signal generated by a cardiac action potential recorded with 1/360 the excitation light used by

Bowmaster et al. [1] was half the amplitude (relative to the noise). Single, unaveraged, action potentials could be resolved with the same lower excitation light intensity. A photodiode was employed for these recordings because the fluorescence intensity was high enough to obviate the use of the photomultiplier tube.

The one additional measure taken to improve the signal-to-noise ratio was rounding the tip of the fiber with a hydrogen torch to create a crude hemispherical lens. The beam diameter of the excitation light was thereby made smaller and, presumably, so was the field of collection. Experiments performed to compare the non-rounded-tip and rounded-tip fibers were performed at the same location in the heart. Fig. 5 illustrates the gain in signal size from rounded-tip fiber. The increased signal is due to reduced baseline fluorescence ( $F$ ) rather than an increased fluorescence change ( $\Delta F$ ).

With the use of the aforementioned changes, to the system a good quality cardiac action potential could be recorded without averaging as illustrated by Fig. 6. The heart that generated this signal was stained with RH237, a rounded-tip 100  $\mu\text{m}$  core fiber was used, and the excitation light intensity was increased by a factor of 10 over the intensity used in Figs. 4 and 5. With the higher light intensity, bleaching of the dye to half fluorescence intensity occurred in 6 minutes.

### Recordings from Lobster Axon:

Numerous attempts were made to record from lobster axons in desheathed circumesophageal connectives with superfused fluorescent dyes (WW781, RH237, RH414). All of the dyes stained and fluoresced strongly, but no action-potential-related signals could be discerned from the noise. Success came with the intracellular injection of the styryl dye RH461. The baseline fluorescence (and noise) was less by a factor of approximately 100, and action-potential-signals could be detected above the noise. Figs. 7a and b illustrate an average of 64 traces from a lobster axon with the dye iontophoretically applied. The recording in Fig. 7b was digitally filtered [15]. The nerve was stimulated with a suction electrode at one end, and the optical fiber was located about 1 mm from the intracellular (dye filled) microelectrode with which the electrical recordings were made (Fig. 7c). The signals are inverted because the dye molecules are bound to the inner membrane so they experience an opposite electric field than when the dye is applied to outer membrane. Dye fluorescence was detected up to 3 mm from the injecting electrode. The excitation light intensity was kept low (as in Figs. 4 and 5) because photodynamic damage at greater intensities caused the action potential to decrease in amplitude (probably due to propagation failure beyond the damaged spot). Dye bleaching did not occur at this intensity since the baseline

fluorescence did not change over 5 minutes; however, the signal size was reduced considerably over that 5 minutes. This may be due to the dye leaving the cell and binding to the outer membrane (Lev-Ram, personal communication). The dye was visible with a fluorescence microscope as shown by Fig. 7d. The dye-fluorescence in this micrograph was only visible to 1 mm from the injection site, even though it could be detected to 3 mm.

## DISCUSSION

Our results show that the technique of optical recording with fluorescent voltage-sensitive dyes can be extended to use with single optical fibers with comparable signal-to-noise ratios as with other techniques. Cardiac action potentials were recorded through a fine optical fiber (with an outer diameter of 140  $\mu\text{m}$ ) without signal averaging. Action potentials from single axons were discerned. One improvement made was employing a 100  $\mu\text{m}$  core fiber rather than the 4  $\mu\text{m}$  core fiber used previously [1]. This allowed 80 times as much fluorescence to be collected which should theoretically improve the signal-to-noise ratio by about a factor of 9 ( $\sqrt{80}$ ). Although the signal-to-noise ratios varied between preparations and locations, we generally saw signal-to-noise ratio improvements of this magnitude.

A second improvement was utilizing green excitation (543 nm) excitation light rather than red (633 nm). The availability and

relatively low-cost, green, helium-neon lasers allowed us to try a variety of styryl dyes that are excitable at this shorter wavelength and can be used at lower concentrations, with less photodynamic damage [6,7]. We also found that the fluorescence spectrum of one of these dyes, when bound to cells, is of short enough wavelength to be optimally detected by a photomultiplier tube. Additionally, calcium-sensitive fluorescent dyes are excitable at the green wavelength [13], and can theoretically be used with this system. Recently, Tung and colleagues [14] have used an optically equivalent system to achieve recordings of high fidelity from frog heart with the voltage-sensitive dye di-4-ANEPPS [8].

A third improvement was rounding the fiber tip. This is probably related to the crude lens narrowing the field of detection and limiting the collection of fluorescence from extraneous fluorescing tissue. The rounded tip has the additional advantage probably being less traumatic when inserted into tissue.

The difficulty in recording from lobster axon and the necessity for intracellular dye injection underscores a limitation intrinsic in using optical fibers. The problem is that fibers have a low collection efficiency as the distance between the fiber and fluorescing tissue increases (fig. 2). Most likely, in the case of bath application of dyes to lobster nerve, non-excitable glial and connective tissue generated most of the background fluorescence (and noise) which obscured the

signal from the more distant axon membrane. With intracellular dye application, only the excitable tissue was stained and thus fluoresced. This is in contrast to frog heart in which a great proportion of the stained tissue is excitable.

This single fiber technique is potentially useful in applications other than those described here. The chief advantage of the fiber technique is that a line-of-sight path is not needed for fluorescence measurements. The fiber is implantable in tissue with relatively little disruption. Light, once entering a fiber, can be carried many meters without attenuation, therefore intracellular optical recording is possible with all of the hardware located remotely from the tissue preparation. We measured fluorescence changes of less than 1% using excitation illumination that did not cause photodynamic damage, and we detected fluorescence that was not visible through a fluorescence microscope. Although we have improved this system considerably, our recordings are still from single sites and are noisier than those made through the optics of a microscope by Salama [16]. These disadvantages must be considered before adopting such a system. Similar fluorescence measurements through optical fibers can, in theory, be applied to any other fluorescent indicator, either physiological or anatomical.

**ACKNOWLEDGMENTS**

The authors thank Ms. Jean Rinaldi for obtaining the fluorescence spectra, Mr. Dean Elbert for preparing the figures, and Mr. Morton Fink for melting the fiber tips. This work was partially supported by an intra-agency agreement (#FDA224-90-6001) to H.J.B..

## REFERENCES

1. Bowmaster, T.A., Davis, C.C. and Krauthamer, V. (1991)  
*Biochemica et Biophysica Acta*. 1091, 9-14.
2. Dalton, J.C. (1958) *J. Gen. Physiol.* 41, 529-542.
3. Dillon, S.M. (1990) *FASEB J.* 4, 682A.
4. Dillon, S. and Wit, A. (1988) *Proc. IEEE-BME* 10, 215-216.
5. Grinvald, A. (1985) *Ann. Rev. Neurosci.* 8, 263-305.
6. Grinvald, A., Hildesheim, R., Farber, I.C. and Anglister, L.  
(1982) *Biophys. J.* 39, 301-308.
7. Grinvald, A., Salzberg, B., Lev-Ram, R. and Hildesheim, R.  
(1987) *Biophys. J.* 51, 643-651.
8. Loew, L.M., Cohen, L.B., Salzberg, B.M., Obaid, A.L. and  
Bezanilla, F. (1985) *Biophys. J.* 47, 71-77.
9. Krauthamer, V., Bekken, M. and Horowitz, J.L. (1991)  
*Bioelectromagnetics* 12, 299-314.
10. Krauthamer, V. and Ross, W. (1984) *J. Neurosci.* 4, 673-682.

11. Kudo, Y., Takeda, K., Hicks, T.P., Ogura, A. and Kawasaki, Y. (1989) *J. Neurosci. Meth.* 30, 161-168.
12. Maynard, D.M. and Walton, K.D. (1975) *J. comp. Physiol.* 97, 215-243.
13. Minta, A., Kao, J. and Tsien, R. (1989) *J. Biol. Chem.* 264, 8171-8178.
14. Neunlist, M., Zou, S. and Tung, L. (1992) *Pflugers Arch.* (in press).
15. Ross, W. and Krauthamer, V. (1984) *J. Neurosci.* 4, 659-672.
16. Salama, G. (1988) *Spectroscopic Membrane Probes*, L. Loew, ed., CRC Press, Inc., Boca Raton, FL.

Table I. Comparison of Fibers. Intensity measurements were made of light emitted from tips of the fibers and returned fluorescence from a solution of voltage sensitive dye (WW781, 1mg/ml) for the three fiber diameters.

Fig. 1. Diagram of Optical Recording System (adapted from [1] with permission).

Fig. 2. Attenuation of Fluorescence with Distance. This is a plot of percentage of maximum fluorescence intensity with distance from a fluorescent surface in air. The plot is shown for fiber core diameters of 4  $\mu\text{m}$ , 50 $\mu\text{m}$  and 100 $\mu\text{m}$ . "A" is plotted on normal axes, and in "B" distance is plotted logarithmically. Measurements were made at 10  $\mu\text{m}$  intervals. The fluorescent intensities have been normalized; the actual magnitudes for the 50  $\mu\text{m}$  and 100  $\mu\text{m}$  fibers were 92 and 450 times the value of the 4  $\mu\text{m}$  fiber. Note that half intensity is reached at distances of 24  $\mu\text{m}$  for the 4  $\mu\text{m}$  fiber, 103  $\mu\text{m}$  for the 50  $\mu\text{m}$  fiber and 95  $\mu\text{m}$  for the 100  $\mu\text{m}$  fiber.

Fig. 3. RH237 Spectra. The top spectrum is from a 38  $\mu\text{M}$  aqueous solution of RH237 in phosphate-buffered saline (PBS). The middle spectrum is from a mouse C-1300 neuroblastoma cell suspension [9] stained with 38  $\mu\text{M}$  of the dye (for 10 minutes) and rinsed with PBS; the fluorescence magnitude is plotted at 1/10 the scale as for the dye in solution (upper spectrum). The bottom spectrum is

of the dye excitation bound to the cells measured at the peak fluorescence of 664 nm. These spectra were made with an SLM Instruments, model SPF 500C, spectrofluorometer (Urbana, IL).

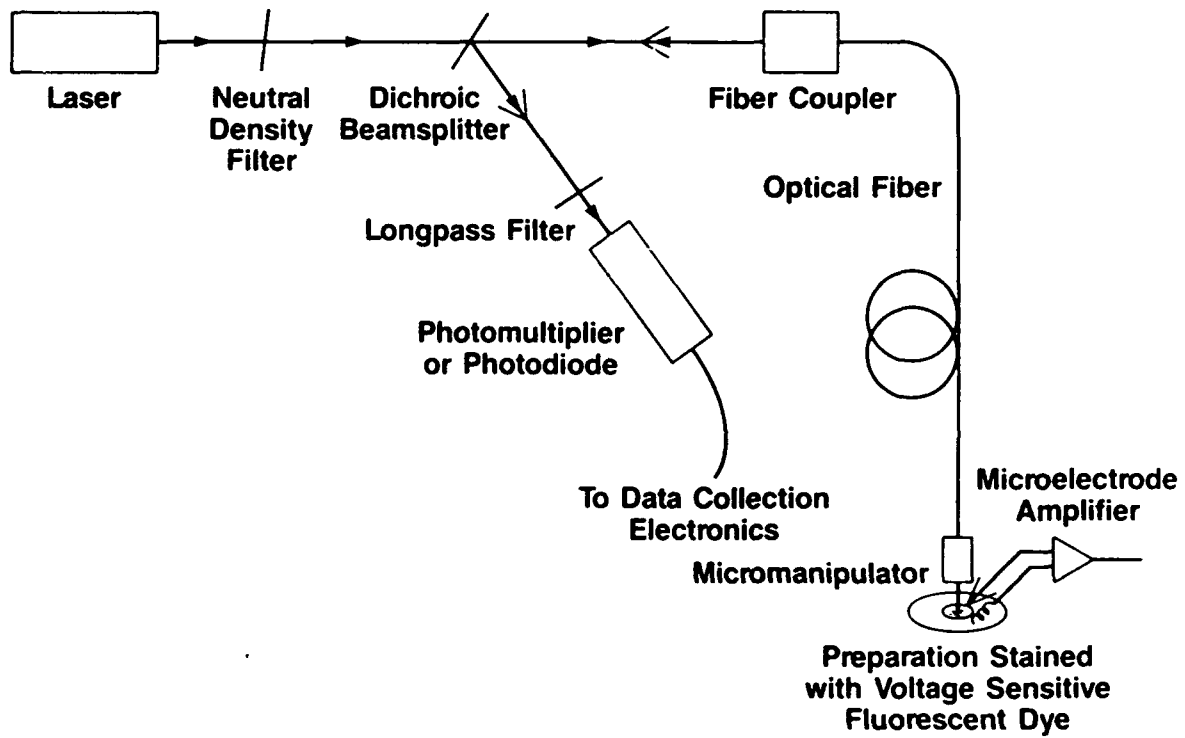
Fig. 4. Cardiac Action Potential. The frog heart was stained with RH237; green (543 nm) excitation, a  $10^{-2}$  neutral density filter and 100  $\mu\text{m}$  core fiber were used. The signals were processed through a passive high-pass filter ( $\tau = 10$  sec), which removed the D.C. component of the signal, and a passive low-pass filter ( $\tau = 1.4$  msec) which removed high frequency noise. "A" shows spontaneously-generated action potentials from the ventricle in calcium-free saline solution. The upper trace is the electrocardiogram (ECG), the lower trace is a single unaveraged optically-recorded action potential, and the middle trace is an average of 10 action potentials that was synchronized from the peak of the QRS wave of the ECG. "B" was recorded in the same manner as "A" from a paced heart with 0.1 mM  $\text{Ca}^{2+}$  present; it shows a movement-related signal (contraction) that occurred 100 msec after the depolarization.

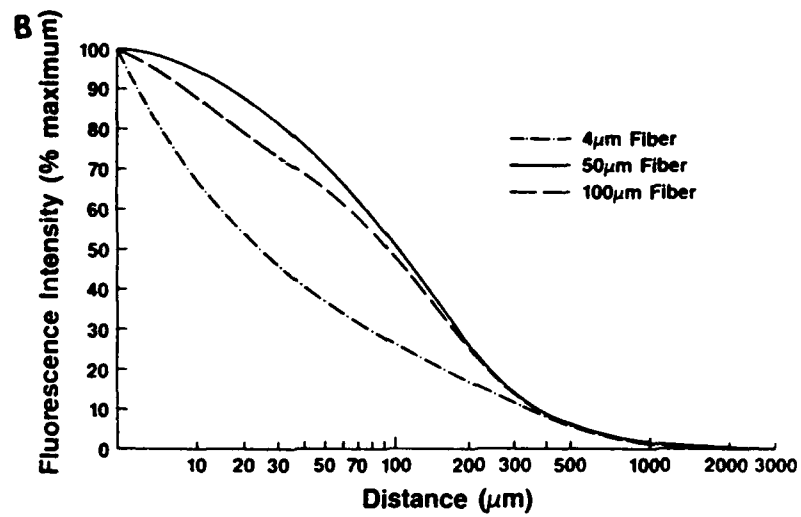
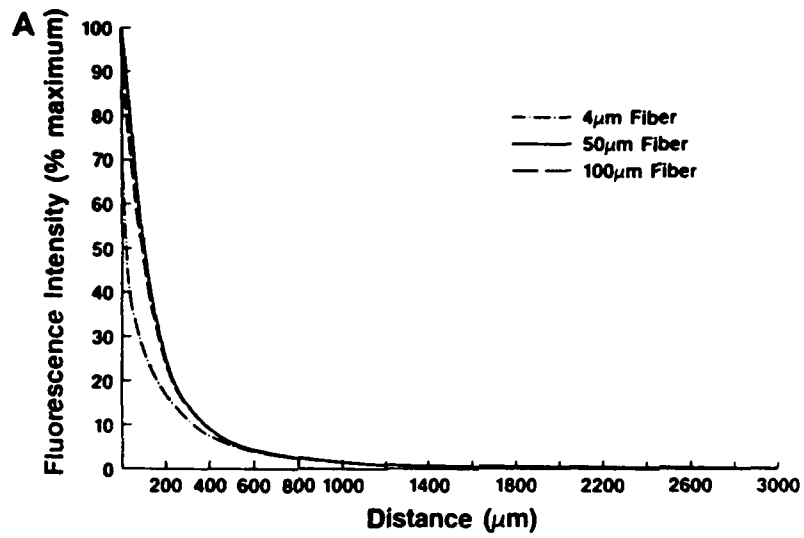
Fig. 5. Lens on Fiber. Rounding the tip of the fiber improved the signal size from the frog heart. The optical recording was performed as in Fig. 3. The upper trace is a single record from a frog atrium detected with a 100  $\mu\text{m}$ -core non-rounded fiber. The lower trace was made 10 minutes later with the rounded-tip fiber from the same spot on the atrium.

Fig. 6. Optimized Recording. This figure depicts a single (unaveraged) action potential from frog atrium. It represents a typical recording employing a 100  $\mu\text{m}$  core fiber with a rounded end and 10 times the light intensity ( $10^{-1}$  neutral density filter) that was used in Fig. 3.

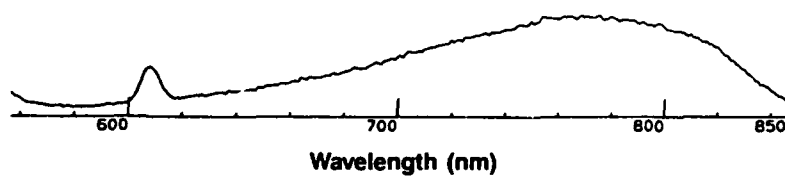
Fig. 7. Axonal Recording. This is an averaged (64 traces) fluorescence recording from a lobster axon stained with the intracellularly injected dye RH461. The same optical arrangement as that used for RH237 was employed here with a  $10^{-2}$  neutral density filter in front of the laser and a non-rounded 100  $\mu\text{m}$ -core fiber. "A" represents the optical data processed through passive RC filters (5 KHz - low pass, 30 Hz - high pass). "B" is that same signal digitally filtered at 1 KHz (Ross and Krauthamer, 1984). "C" is an intracellular microelectrode recording made 1 mm distal from the optical recording site. The fluorescence micrograph ("D") was made of the axon following recording. Note that the dye appears bound to the membrane. The fluorescence recordings in "A" and "B" appear inverted because the dye was applied to the inner membrane as opposed to the outer membrane as in the other figures.

Fiber Core Diameter	Emitted Light	Returned Fluorescence	Returned Fluorescence/ Emitted Light
4 $\mu\text{m}$	1.00	1.0	1.0
50 $\mu\text{m}$	2.55	82.1	32.2
100 $\mu\text{m}$	2.84	227.9	80.2

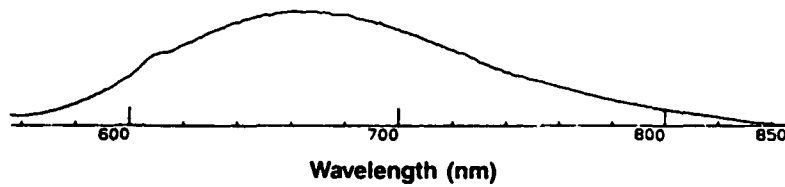




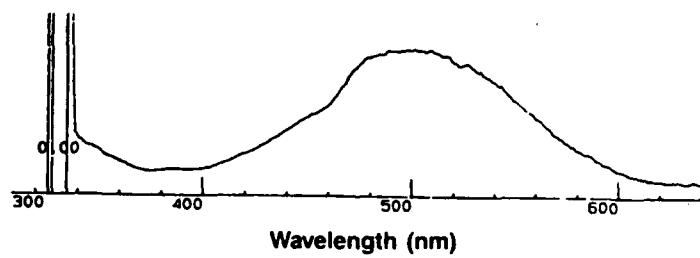
**Fluorescence in Solution (543 nm Excitation)**

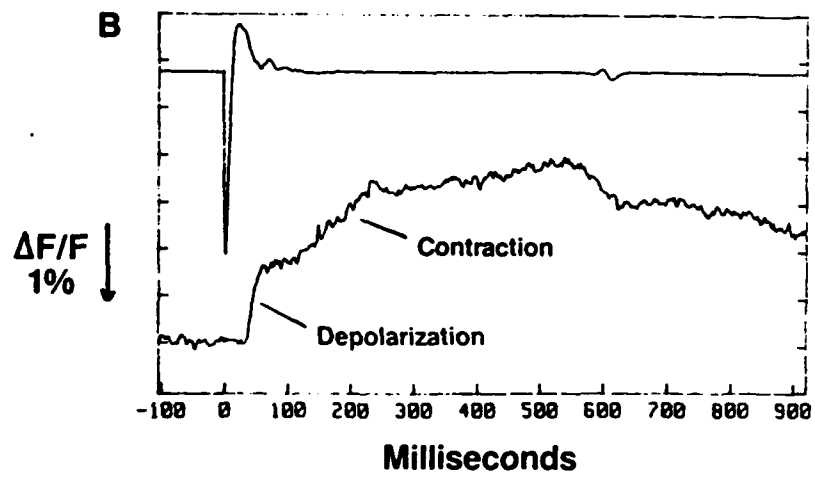
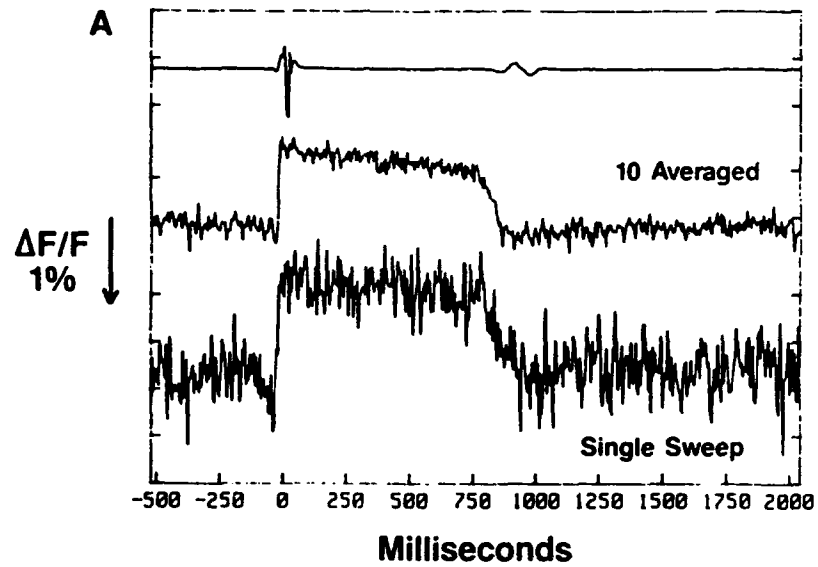


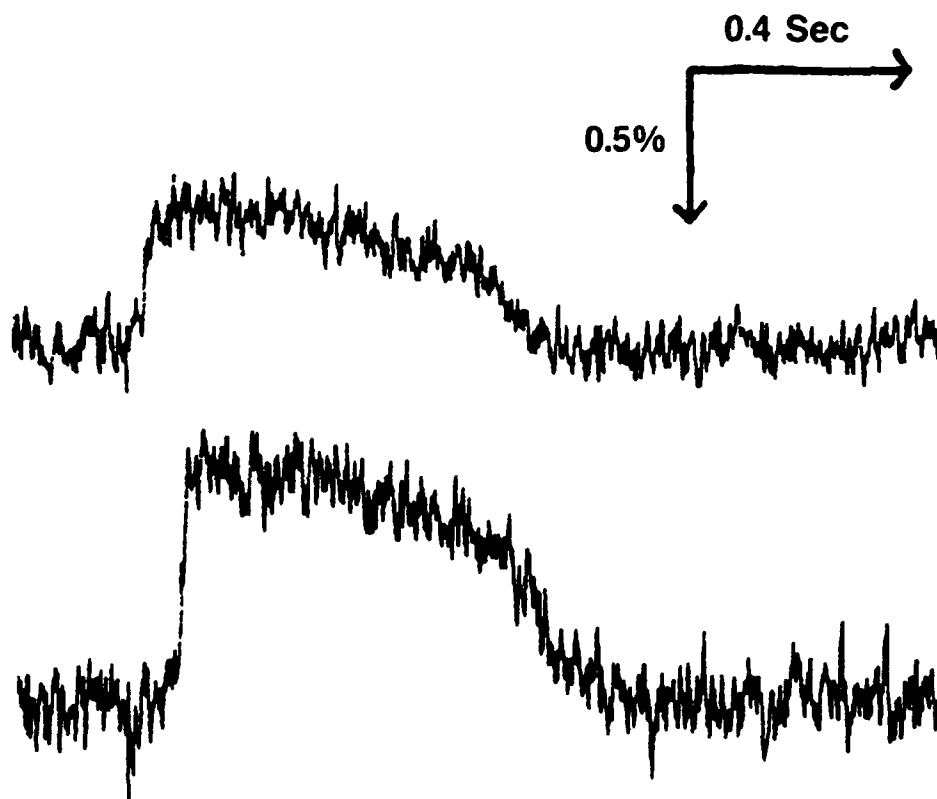
**Fluorescence With Cells (543 nm Excitation)**

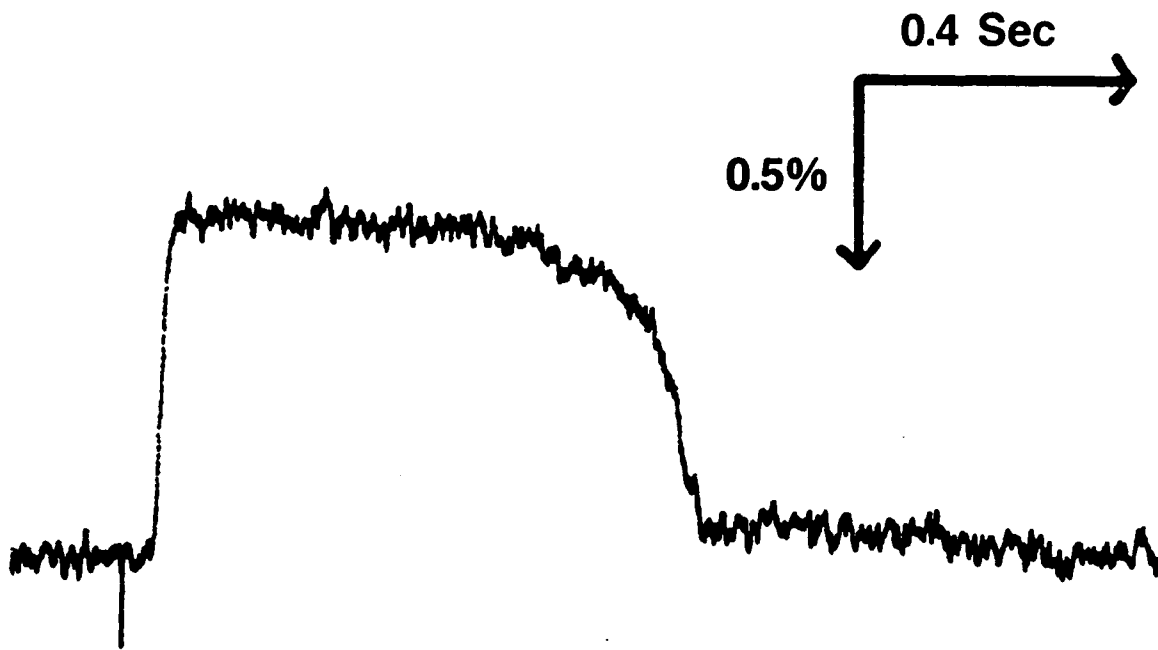


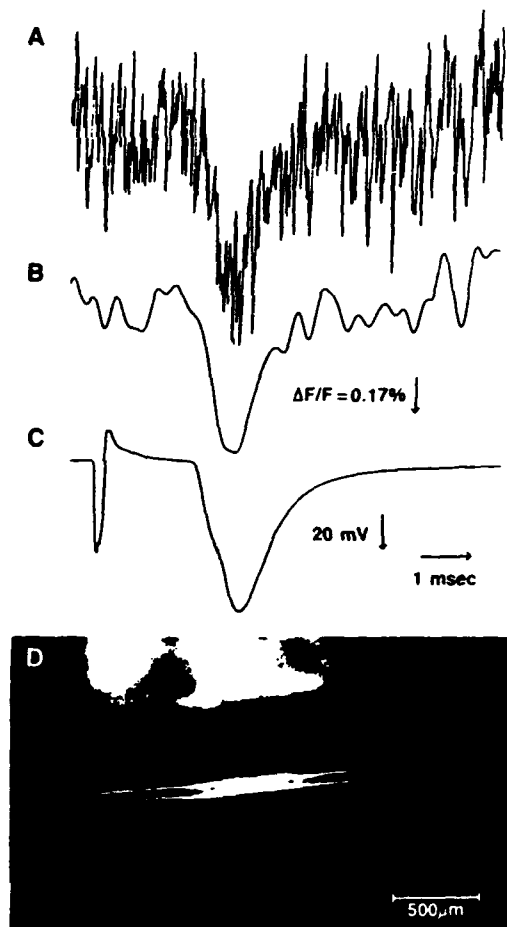
**Excitation With Cells (664 nm Fluorescence)**











# Hybrid fiber-optic sensor using true heterodyne measurement techniques

David L. Mazzoni, Kyuman Cho, and Christopher C. Davis

Department of Electrical Engineering, University of Maryland, College Park, Maryland 20742

Received January 14, 1991; accepted January 29, 1991

We describe a hybrid, coherent, fiber-optic sensor for the measurement of phenomena that lead to birefringence, polarization rotation, or differential phase shifts in a remote-sensing element. By utilizing a single fiber that carries two orthogonally linearly polarized laser beams of different frequencies to the sensor and true heterodyne detection, we obtain high common-mode rejection of any unwanted intrinsic sensitivity of the fiber itself. The sensor is resistant to fading and has a high dynamic range. For demodulation we use high-frequency phase-locked loop detection that is insensitive to slowly varying phase shifts.

Fiber sensors are ideal for the remote sensing of parameters in hostile environments or where electromagnetic fields can interfere with traditional sensors.<sup>1,2</sup> Coherent fiber sensors detect phase or polarization changes induced in the fiber itself (intrinsic sensors) or in a sensing element interrogated through the fiber (a hybrid sensor) by using some interferometric or optical heterodyne scheme. Coherent sensors are generally more complex than incoherent ones but have potentially much greater sensitivity. A potentially important application of coherent sensors is in the *in vitro* (or *in vivo*) monitoring of the electrical activity of biological cells and tissue.<sup>3</sup> In this, and many other applications, to be practicable the sensor must be made single ended. The fiber must carry both signal and reference beams to and from a remote location where the desired phenomenon is sensed.

In our coherent hybrid sensor we have combined two orthogonally polarized beams into a single fiber, thereby minimizing common-mode effects. In addition, to avoid the operating point drift that plagues homodyne detection schemes, we have used a true heterodyne scheme in which these two orthogonally polarized beams are at different frequencies. A single monomode fiber acts to deliver and return the beams to and from a remote sensor element. The remotely located sensing element changes the phase or relative polarization state of the two beams, which are then reflected back into the fiber. The detection optics and electronics can be located in a benign location at the input end of the fiber, where environmental interference can be controlled. This type of single-fiber system is less vulnerable to its environment, since perturbations affect both beams in the fiber and common-mode signals can be suppressed in the detection electronics.

Interferometric fiber sensors, and interferometers in general, are sensitive to the relative phase difference between the signal and reference arms.<sup>4-8</sup> The polarization state at the output of the sensor must also be maintained for optimum mixing of the two interferometer beams. Slow, uncorrelated changes in the length, the birefringence, or the orientation of the fi-

ber or the optical components must somehow be compensated for, or the system must be designed to be insensitive to them. Schemes employing fiber squeezers, rotators, Faraday cells, and other techniques have been investigated with some success.<sup>7-9</sup> We have avoided these complicated approaches by using a phase-locked loop demodulation scheme that is not sensitive to slowly varying phase drift. Moreover we have minimized polarization state changes in the fiber by using two orthogonally polarized beams in a single fiber. Our present system shows no signal fading problems for fiber lengths of up to several meters. For longer lengths of fiber an input polarization controller could be used to maintain optimal demodulation conditions.

Practical details of our fiber sensor are given in Fig. 1. With a KD\*P crystal as the remote-sensing element, the local electric field modulates the birefringence of the crystal. This induces a phase shift that can be detected by placing the output polarization-sensitive beam splitter PSBS2 at 45°. If a Faraday cell is used as the remote-sensing element, rotation of polarization occurs that is modulated by the local magnetic field. To detect the modulation that results from this rotation of polarization, the output PSBS2 is aligned with the initial polarizations. This is done by adjustment of the  $\lambda/2$  plate in front of PSBS2. Vibration measurements can be made by placing a PSBS, a  $\lambda/2$  plate, and a mirror at the end of the fiber as shown in Fig. 2. In vibration measurements a phase shift is incurred owing to the differing path lengths, and detection is similar to that of the first method just outlined. Finally, detection of the signal that returns from the sensing element occurs at a balanced mixer using two wideband photodiodes.

If the fiber has significant circular birefringence that is not compensated for by polarization control at the launch end of the fiber, then under worst-case conditions significant signal fading can occur. However, the signal can always be recovered and the detectors brought back into balance by rotating the  $\lambda/2$  plate in front of PSBS2. For example, optimal phase detection occurs when the two orthogonal polarization

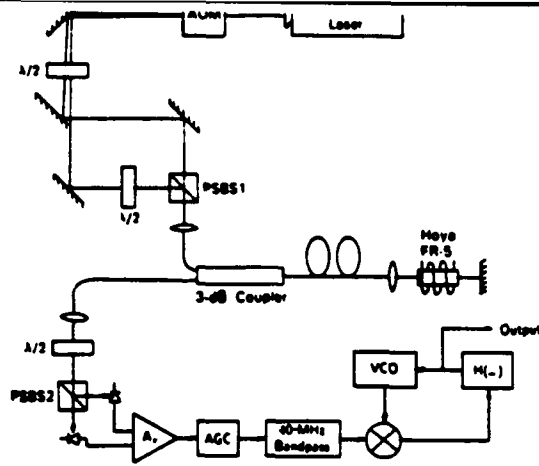


Fig. 1. Experimental arrangement for the hybrid fiber-optic probe. The two  $\lambda/2$  plates encountered after the acousto-optic modulator (AOM) orient the 40-MHz separated beams with the first polarization-sensitive beam splitter (PSBS1). The combined beams are launched into a single-mode fiber (SMF) with a 3-dB coupler at the launch end. The beam returning from the sensing stage, which in this case is a magnetic-field sensor that uses Faraday-active glass, is directed through a  $\lambda/2$  plate onto PSBS2. Amplitude and phase modulation can be detected by the orientation of the beams on PSBS2. A phase-locked loop is used to demodulate the signal information.

states emerging from the fiber are oriented at  $45^\circ$  to the axes of the PSBS. Complete fading of the signal can occur if the two orthogonally polarized signals separated by 40 MHz emerge linearly polarized parallel to the axes of the PSBS. In practice, we have not had such problems associated with bending or twisting of the fiber in the sensor described here. Linear birefringence of the fiber can lead to pseudostatic phase differences, which the phase-locked loop (PLL) automatically tracks out of the demodulated signal.

Our sensor arrangement differs from previously reported coherent fiber sensor schemes in its use of two orthogonally linearly polarized, frequency-shifted laser beams, a single monomode fiber, which does not need to be a high-birefringence type, and true heterodyne demodulation. The extrinsic magnetic field sensor described by Tatum and Jackson<sup>10</sup> comes closest to our scheme. However, these authors use a pseudoheterodyne scheme with two orthogonally polarized beams in high-birefringence fibers and multiple fibers to return optical signals to their detectors. Chandler *et al.*<sup>1</sup> also use a double-frequency scheme in a single fiber, but their sensor is an intrinsic one in which circularly polarized eigenmodes are used in circularly birefringent fiber.

A general representation for our detection scheme can be written as

$$\begin{bmatrix} E_1 \\ E_2 \end{bmatrix} = \begin{bmatrix} \cos \theta & -\sin \theta \\ \sin \theta & \cos \theta \end{bmatrix} \times \begin{bmatrix} A & -B \\ B & A \end{bmatrix} \begin{bmatrix} E_x \exp(i\omega t + \phi_x) \\ E_y \exp(i\omega' t + \phi_y) \end{bmatrix}, \quad (1)$$

is the Jones matrix for a PSBS, followed by the matrix for a medium with linear and circular birefringence.<sup>11</sup> For simplicity, if we neglect fiber effects, then the first and second matrices in Eq. (1) can be written as in the second column of Fig. 2.

For linear birefringence measurements, the output of the differential amplifier is

$$I_{\text{diff}} \propto |E_2|^2 - |E_1|^2 = 2E_x E_y \cos(\Delta\omega t + \Delta\phi_s - \phi_m), \quad (2)$$

where  $\Delta\omega = \omega - \omega'$  is the AOM excitation frequency,  $\phi_m$  is the induced phase shift, and  $\Delta\phi_s = \phi_x - \phi_y$  is the static phase term. In an electrical homodyne demodulation scheme,  $\phi_m$  is measured by mixing the detected signal with a portion of the AOM excitation. The output from the mixer after low-pass filtering can be written as

$$I_{\text{diff}} \propto E_x E_y \cos(\phi_m - \Delta\phi_s).$$

Optimum demodulation of  $\phi_m$  is achieved when  $\Delta\phi_s = (2n + 1)\pi/2$ . For long-term stability, this condition should be maintained by feedback control.

The  $\Delta\phi_s$  term in relation (2) represents a static phase shift due to differing path lengths, thermal expansion and contraction of the optical components, and other slowly varying effects. This term includes intrinsic effects in the fiber such as slowly varying circular or linear birefringence. Heterodyne detection is immune to these pseudostatic phase perturbations. In our current sensors of this kind we do not observe significant slowly varying phase changes attributable to such effects, but their occurrence would mask low-frequency real signals from the sensor. Therefore this configuration is not a good sensor for small dc effects.

Magnetic fields and other phenomena that cause rotation of polarization can be sensed by using the second scheme in Fig. 2. In this case PSBS2 is oriented in the same plane as PSBS1. Difference detection is used to yield the output signal

Detection Schemes	Jones Matrix	Sensitivity
	$\begin{pmatrix} e^{i2\phi} & 0 \\ 0 & e^{-i2\phi} \end{pmatrix}$	$44.5 \cdot 10^{-6} \frac{\text{rad}}{\sqrt{\text{Hz}}} (11^\circ/\text{m})$
	$\begin{pmatrix} \cos \theta & -\sin \theta \\ \sin \theta & \cos \theta \end{pmatrix}$	$37.4 \cdot 10^{-6} \frac{\text{rad}}{\sqrt{\text{Hz}}} (2.6 \mu\text{T})$
	$\begin{pmatrix} e^{i2\phi} & 0 \\ 0 & e^{-i2\phi} \end{pmatrix}$	$3.3 \cdot 10^{-11} \frac{\text{m}}{\sqrt{\text{Hz}}}$

Fig. 2. Detection schemes and sensitivities. Different remote-sensing methods are shown schematically in the left column, with a simplified Jones matrix for the respective scheme in the center column. The sensitivities listed are those actually obtained with the sensor at a frequency of 100 Hz.

$$I_{\text{diff}} = |E_2|^2 - |E_1|^2 = 2E_0^2 \sin 2\theta_F \cos(\Delta\omega t + \Delta\phi_s), \quad (3)$$

where the rotation angle is

$$\theta_F = VIB_0 \sin \omega_m t,$$

with  $V$  the Verdet constant.

The phase modulation in relations (2) and (3) is usually demodulated by either homodyne or heterodyne detection.<sup>4</sup> Under ideal conditions homodyne detection gives the largest detected signal. However, owing to pseudostatic drift a feedback system is required to maintain the output signal level. Homodyne feedback systems of this sort have the drawback that they eventually run out of control range and must be reset. This reset problem can be avoided by using a heterodyne detection scheme.

In heterodyne detection the diode output phase is commonly detected with a FM discriminator or a PLL. This can be done with commercial 455-kHz FM components in a superheterodyne mode<sup>12</sup> or by direct PLL detection at the carrier frequency. The direct detection method does not require a stable source since a voltage-controlled oscillator is locked to the carrier. A doubly balanced mixer can be used rather than the digital phase detector common to commercial PLL chips, which lack the phase sensitivity needed for extremely sensitive detection. Although other schemes exist for heterodyne detection,<sup>7</sup> they often require complicated techniques and are usually not so sensitive as true heterodyne methods.<sup>9</sup>

The simplicity of the detection electronics with the direct PLL method is evident from Fig. 1. Balanced detection is used to suppress amplitude noise from the laser. In Fig. 1 the phase modulation is detected in a discrete 40-MHz PLL that uses a limiter/automatic gain control (AGC), a doubly balanced mixer, a 40-MHz voltage-controlled oscillator (VCO), and an active loop filter. Phase demodulation is achieved by mixing the differential amplifier output with the VCO output. The VCO control voltage contains the demodulated phase signal, which is further amplified before the output signal is displayed on an oscilloscope or dynamic signal analyzer. This detection scheme is elegant and does not require any specialized or expensive components, which makes the sensor desirable for commercial applications.

The phase sensitivity that we have achieved in the true heterodyne mode with this sensor is  $7 \mu\text{rad}/\sqrt{\text{Hz}}$  at 100 Hz with a power at the photodiodes of 50  $\mu\text{W}$ . This is a factor of 40 above the photon noise limit with this power. The corresponding electric-field, magnetic-field, and vibrational sensitivities that we have achieved are summarized in Fig. 2. If we use homodyne demodulation, then we achieve a sensitivity of  $\sim 0.7 \mu\text{rad}/\sqrt{\text{Hz}}$ , close to the photon noise limit. All these sensitivities represent state-of-the-art values for coherent extrinsic fiber sensors. These sensitivities obtained at a low detection frequency demonstrate

stable performance under noisy operating conditions. If we operate our sensors to detect higher-frequency phenomena, where environmental disturbances and  $1/f$  noise are reduced, our sensitivities increase markedly, e.g., by  $\sim 10$  dB in the heterodyne mode for signals at 6 kHz. The power loss from source to detectors that we suffer results from the combination of bulk-optical elements and single-mode fiber that is used. The sensing elements themselves involve bulk-optical elements, and there is substantial power loss in the beams' leaving the fiber, interacting with the sensing element, and returning into the fiber. The remote-sensing elements used for these measurements were composed of discrete components that themselves add noise and reduce performance, but these assemblies can be integrated onto the end of the fiber. We are in the process of integrating all our bulk optics into pigtailed assemblies to minimize power loss. Since single-mode He-Ne lasers are limited to low power levels, in order to increase sensitivity a single-mode diode-pumped 1.33- $\mu\text{m}$  Nd:YAG laser should be an attractive signal source in future versions of this hybrid, coherent sensor scheme.

This research was partially supported by the National Science Foundation through Grant ECS-8906120.

## References

1. G. I. Chandler, P. R. Forman, F. C. Jahoda, and K. A. Klare, *Appl. Opt.* **25**, 1770 (1986).
2. P. R. Forman and F. C. Jahoda, *Appl. Opt.* **27**, 3088 (1988).
3. C. C. Davis, T. A. Bowmaster, and V. Krauthamer, in *Proceedings of the Eleventh Annual Conference of the IEEE Engineering in Medicine and Biology Society* (Institute of Electrical and Electronics Engineers, New York, 1989), pp. 1194-1195.
4. M. Martinelli, in *Optical Fiber Sensors*, A. N. Chester, ed. (Nijhoff, Dordrecht, The Netherlands, 1987), pp. 309-319.
5. A. D. Kersey, A. Dandridge, and A. B. Tveten, in *Digest of Optical Fiber Sensors* (Optical Society of America, Washington, D.C., 1988), Vol. 2, Pt. 1, pp. 44-47.
6. D. W. Stowe, D. R. Moore, and R. G. Priest, *IEEE J. Quantum Electron.* **QE-18**, 1644 (1982).
7. T. Okoshi, *IEEE J. Lightwave Technol.* **LT-3**, 1232 (1985).
8. Y. H. Cheng, T. Okoshi, and O. Ishida, *IEEE J. Lightwave Technol.* **7**, 368 (1989).
9. I. M. I. Habbab and L. J. Cimini, Jr., *IEEE J. Lightwave Technol.* **6**, 1537 (1988).
10. R. P. Tatum and D. A. Jackson, *Opt. Commun.* **72**, 60 (1989).
11. W. J. Tabor and F. S. Chen, *J. Appl. Phys.* **40**, 2760 (1969).
12. S. P. Bush, D. L. Mazzoni, K. Cho, and C. Davis, in *Proceedings of the IEEE Lasers and Electro-Optics Society Annual Meeting (IEEE Lasers and Electro-Optics Society, Piscataway, N.J., 1989)*, p. 267.

**MEASUREMENT OF THE LOCAL SLOPE OF A SURFACE  
BY VIBRATING SAMPLE HETERODYNE INTERFEROMETRY:  
A NEW METHOD IN SCANNING MICROSCOPY**

**Kyuman Cho, David L. Mazzoni,  
and Christopher C. Davis**

**Electrical Engineering Department  
University of Maryland  
College Park, MD 20742  
Tel (301)405 3637**

**Abstract**

**A heterodyne interferometer that uses a vibrating sample has been constructed for surface diagnostics. This interferometer provides a detailed profile of the local slope and/or roughness of a surface. A complete 3-D image of a surface can be obtained.**

There have been several reports of efforts to use interferometric schemes in microscopy<sup>1-5</sup>. Laser homodyne and heterodyne interferometry can measure extremely small displacement changes<sup>6</sup>. In a scanning microscopy application this should allow detailed mapping of surfaces with ultra-fine depth resolution.

Matthews et al.<sup>2</sup> and Suzuki et al.<sup>3</sup> have demonstrated the potential of optical homodyne interferometry in 3D microscopy. The optical path length of the reference arm of the interferometer in these experiments was actively controlled to maintain the interferometer at maximum phase sensitivity. The error signal from a feedback control loop was monitored while scanning the surface<sup>2</sup> to obtain its 3D structure. Unfortunately, this method is extremely sensitive to environmental disturbances: any thermal and acoustic change in optical path length of the interferometer arms can disturb the measurement. Huang<sup>1</sup> was able to overcome these difficulties by the use of a double beam heterodyne interferometer with common-mode rejection that allowed a depth resolution of 10pm.

An optical heterodyne interferometric scheme was proposed by See et al.<sup>4</sup> In their experiment the probe beam was periodically displaced at 1.7 MHz and the phase of the probe beam was modulated by depth variations. These depth variations were converted into intensity contrast on a CRT display. In this way they were able to identify the grain boundaries on a polished stainless steel surface. Although they achieved phase sensitivity close to the photon noise limit, because of the wide noise bandwidth (30 kHz) and small probe power (50  $\mu$ W), the maximum differential depth resolution obtained was  $\sim$ 10pm. Moreover, because the amplitude of the displacement was approximately the size of the focus, the spatial resolution was relatively poor compared to other microscopy techniques.

In this paper we present a more versatile and high resolution microscopy technique that uses a heterodyne interferometer<sup>7</sup>. By using direct phase locked loop RF demodulation we are able to narrow the bandwidth of the measurement, which gives almost two orders of magnitude improvement in average depth resolution compared to that achieved by See et. al. By applying a small amplitude lateral vibration to the object under test (typically

a few nm at 1 kHz), we are able to determine the local slope of its surface. We will call this technique scanning coherent slope microscopy (SCSM).

The heterodyne interferometer used in this research is shown in Fig. 1. Light from a single frequency He-Ne laser is split into two paths by an acousto-optic modulator. The deflected beam suffers a 40 MHz frequency shift and is used as the local oscillator of the interferometer. After the beam splitter BS the other beam (the probe beam) is focused onto the surface under test by a 10X microscope objective (N.A. 0.25). The surface is laterally vibrated by a PZT driven stage. The amplitude of the displacement is  $\sim 5$  nm. The probe beam is phase modulated by this sinusoidal lateral vibration of the surface. Since the focused beam has a finite size, the modulation depth is determined by the geometrical average of the pathlength (GAPL) over the focused region. The GAPL difference caused by the small amplitude vibration of the surface is a measure of the local slope. The lateral spatial resolution is thereby limited by the focusing optics, because surface roughness smaller than the focal spot is averaged. The reflected beam from the surface is collected by the focusing lens and sent back to the BS. The local oscillator and probe beams are combined in the BS and mixed at the photodiode PD. The phase modulation on the probe beam is then carried by the RF intermediate frequency. The signal current  $i_s$  from the photodiode is

$$i_s \propto |E_L|^2 + |E_S|^2 + 2|E_L||E_S|\cos(\Delta\omega t + \Delta\phi), \quad (1)$$

where  $\Delta\omega$  is the RF intermediate frequency and  $\Delta\phi$  is the phase difference between the probe and local oscillator beams. The phase term can be rewritten as

$$\Delta\phi = \phi_m + \phi_s, \quad (2)$$

where  $\phi_m$  is the sinusoidally modulated phase term and  $\phi_s$  represents other environmentally induced phase changes caused by thermal drifts of the optical paths and acoustic vibrations of optical components. If the surface is displaced in the  $x$ -direction with a small

displacement  $\delta x = \delta_o \sin \omega_m t$ , the resulting optical path length change is

$$\delta z \approx \alpha \delta x = \alpha \delta_o \sin \omega_m t, \quad (3)$$

where  $\delta_o$  and  $\omega_m$  are the amplitude and frequency of the displacement, and  $\alpha = \delta z / \delta x = \tan \theta$ , is the local slope of the surface. The above equation is a good approximation for small displacements because the path length change caused by the reflection angle difference is negligible. The modulated phase term is then given by

$$\begin{aligned} \phi_m &= \frac{4\pi}{\lambda} \delta z \\ &= \frac{4\pi}{\lambda} \alpha \delta_o \sin \omega_m t \end{aligned} \quad (4)$$

This sinusoidally modulated phase term can be detected by using a phase locked loop. After a high pass filter, the RF signal from the photodiode is mixed with a RF local oscillator derived from a voltage controlled oscillator (VCO). The intermediate frequency output from the mixer passes through a loop filter and is used as an error signal to drive the VCO. The VCO is frequency locked to the RF input signal and the time variation of the phase term can be measured from the VCO driving signal. Since this scheme is not sensitive to a quasi-static phase change, it does not require feedback control of the optical path length of the interferometer. Moreover, since the signal from the phase locked loop is synchronously detected by a lock-in amplifier, any unsynchronized background disturbance of the interferometer is filtered out.

The sensitivity of a heterodyne interferometer has been calculated by many authors<sup>8</sup>. If a temporally and spatially coherent source is used, then the minimum detectable phase difference between the two interferometer arms is

$$\Delta \phi_{\min} = \sqrt{\frac{h\nu \Delta f}{24\eta P}}, \quad (5)$$

where  $P/h\nu$ ,  $\Delta f$ , and  $\eta$  represent the number of photons, detection bandwidth, and quantum efficiency of the photodiode, respectively. The sensitivity calculation has been performed by assuming: (1) 50 % conversion efficiency of the acousto-optic modulator, (2) half of the probe beam is lost at the BS, and (3) there is a 3 dB loss in signal at the RF mixing stage. For a 1 mW He-Ne laser and silicon photodiode ( $\eta \sim 0.8$ ), the minimum detectable phase difference is  $\Delta\phi_{\min} \sim 5 \times 10^{-7} \text{ rad.} \sqrt{\text{Hz}}$ , or equivalently  $\Delta l_{\min} = 2.5 \times 10^{-14} \text{ m} \sqrt{\text{Hz}}$ . In our experiment the equivalent noise bandwidth has been determined by the integration time constant of the lock-in amplifier. For a 10 msec. time constant,  $\Delta f = 1/(8\tau) = 12.5 \text{ Hz}$ . With these parameters, the theoretical limit of the average differential depth resolution is  $\Delta l_{\min} = 8.8 \times 10^{-14} \text{ m}$ .

A complete map of the local slope of a test sample can be determined by scanning the probe over the surface, and the surface structure can be regenerated from this map. In our experiments the test sample was mounted on a PZT driven stage that was itself mounted on a motor driven X-Y stage. The X-Y stage and the lock-in amplifier were interfaced with a personal computer (PC). While scanning the sample over the region of interest, the local slope at each data point was obtained by a standard numerical integration algorithm (cf: Fig. 2).

Fig. 3.(a) shows a scan of an aluminum mirror surface on which a cross-shaped scratch and a series of point indentations were deliberately made. The corresponding scanning electron microscope (SEM) image of the scratch is shown in Fig. 3.(b). A high resolution SCSM image of the cross is shown in Fig. 4. Although in its present form SCSM cannot compete with SEM in lateral resolution, its average depth resolution is much better and depth profiles viewed at different angles are obtained directly. Moreover, the SCSM is non-destructive, since it does not require a conducting surface, and the sample does not need to be sliced to quantify the depth of the image.

It should be noted that the SCSM results shown in Figs. 3 and 4 are 2-D maps of 1-D slope data. Although these maps show qualitative features of the surface, in order to

obtain quantitative images the slope data need to be converted to a depth profile. To date, we have not generated such quantitative images. In Figs. 3 and 4 the slope data was obtained unidirectionally and the data was not calibrated for scattering loss of the probe beam on the scratch. Such scattering loss on the scratch can be compensated by adding an automatic RF gain control stage, and a two dimensional slope vector can be obtained by adding another PZT translation stage that provides lateral vibration in an orthogonal direction.

In this paper we have introduced a heterodyne interferometer that can be used in surface diagnostics. The interferometer has been designed to measure the local slope of a surface. Using this technique we have been able to image the 3D surface structure of various optical components such as lenses and mirrors. SCSM has the following desirable features:

- (1) The microscope is non-destructive.
- (2) The microscope can produce diffraction-limited 3D images of a surface with an average differential depth resolution  $\sim 2.5 \times 10^{-14}$  m.
- (3) With longer scanning times a high resolution image of an entire surface can be obtained. These images can be viewed at different angles with different magnifications using computer graphics so both macroscopic and microscopic diagnostics can be performed on the same data set.

The scanning speed of the current arrangement was determined by the motor driven X-Y stage. With these stages 110x100 data points were obtained in approximately 5 minutes. We believe the scanning time will be significantly reduced by using a long travel PZT driven stage. The scanning speed is then determined by the integration time constant of a lock-in amplifier.

This research was supported by the US Army through contract DAMD17-90-Z-0052. We acknowledge helpful discussions with Professor Marshall Ginter.

## References

- (1) C-C. Huang, Opt. Eng. **23**, 365 (1984).
- (2) H. J. Matthews, D. K. Hamilton, and C. Sheppard, Appl. Opt. **25**, 2372 (1986).
- (3) T. Suzuki, O. Sasaki, K. Higuchi, and T. Maruyama, Appl. Opt. **30**, 3623 (1991).
- (4) C. W. See, M. Vaez Iravani, and H. K. Wickramasinghe,
- (5) H. K. Wickramasinghe, Proc. SPIE **897**, 3 (1988). Appl. Opt. **24**, 2373 (1985).
- (6) C. C. Davis, Nuc. Phys. **B6**, 290 (1989).
- (7) D. L. Mazzoni, K. Cho, and C. C. Davis, Opt. Lett. **16**, 614 (1991).
- (8) M. J. Collet, R. Loudon, and C. Gardiner, J. Mod. Opt. **34**, 881 (1987).
- (9) M. P. Kothiyal and R. S. Sirohi, Appl. Opt. **31**, 75 (1992).

### Figure Captions

**Fig. 1 Experimental Arrangement.** In the figure, OI - optical isolator, AOM - acousto-optic modulator, BS - beam splitter, PD - photodiode, BPF - band pass filter, and VCO - voltage controlled oscillator.

**Fig. 2 Phase modulation caused by lateral vibration of a curved surface.**

**Fig. 3(a) Low resolution SCSM image of a scratched and indented region on an aluminum coated mirror.**

**Fig. 3(b) Corresponding SEM image of Fig. 4(a).**

**Fig. 4 A high resolution SCSM image of a cross-shaped scratch mark on an aluminum coated mirror.**

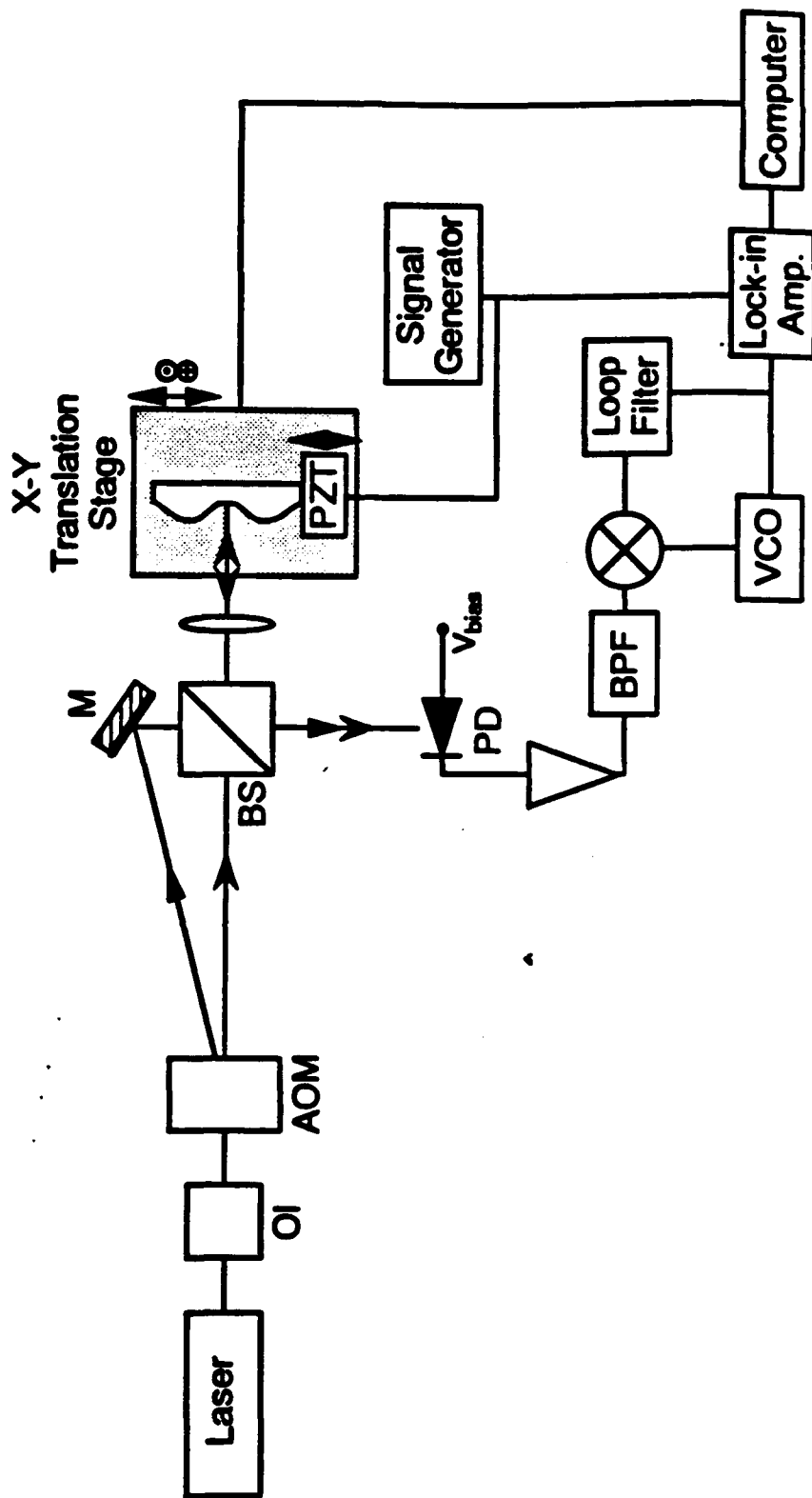


Fig. (1)

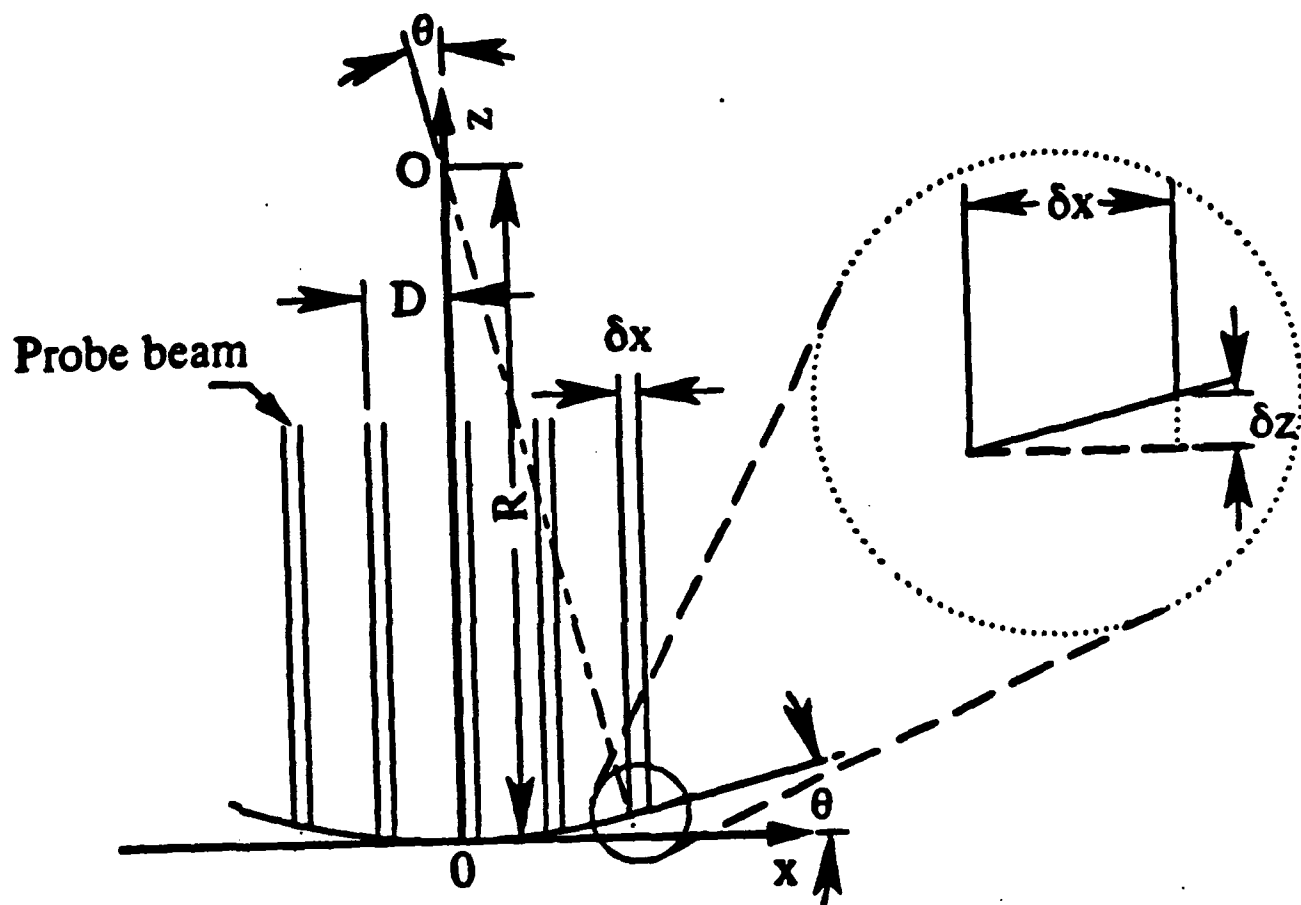


Fig. (2)

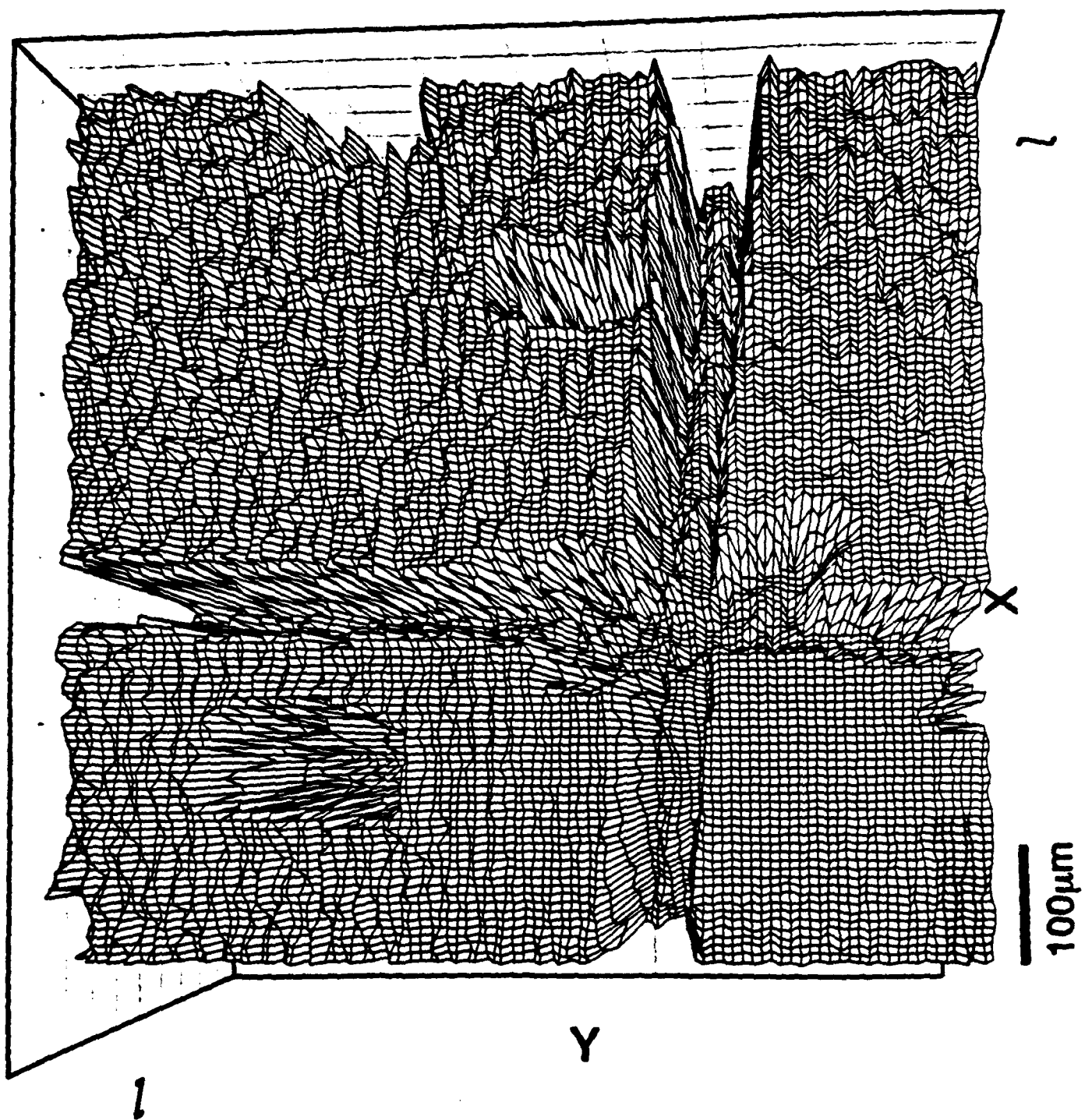


Fig. (3a)

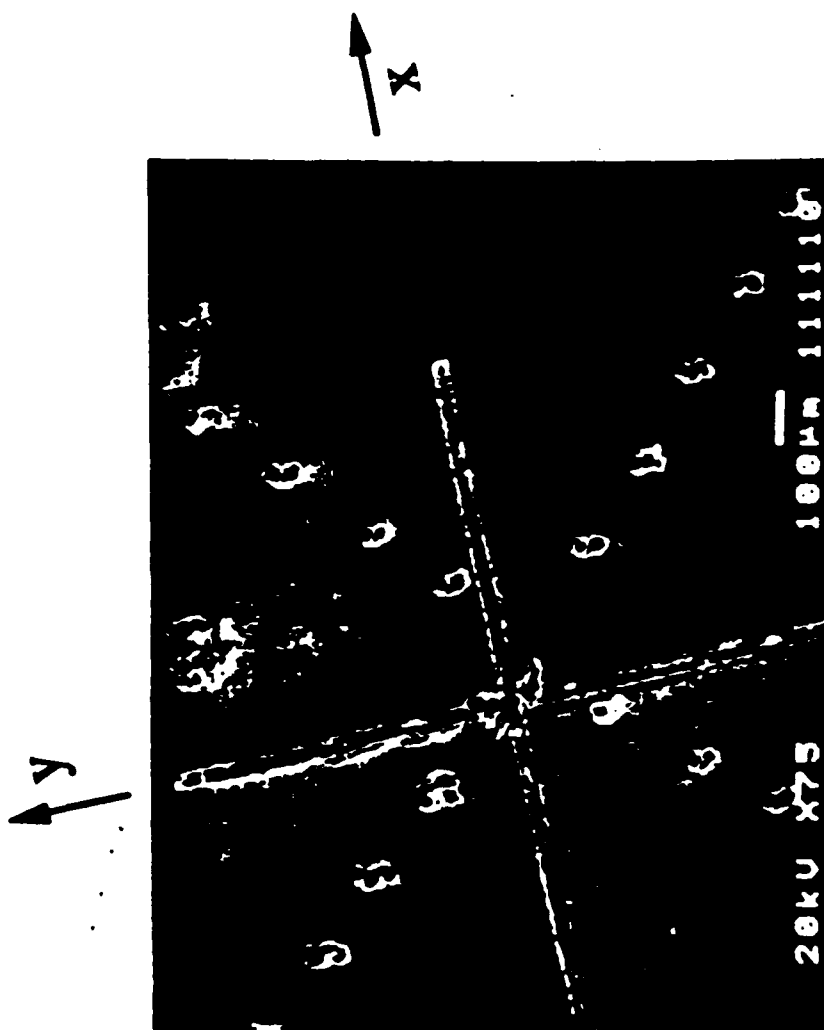


Fig. (3b)

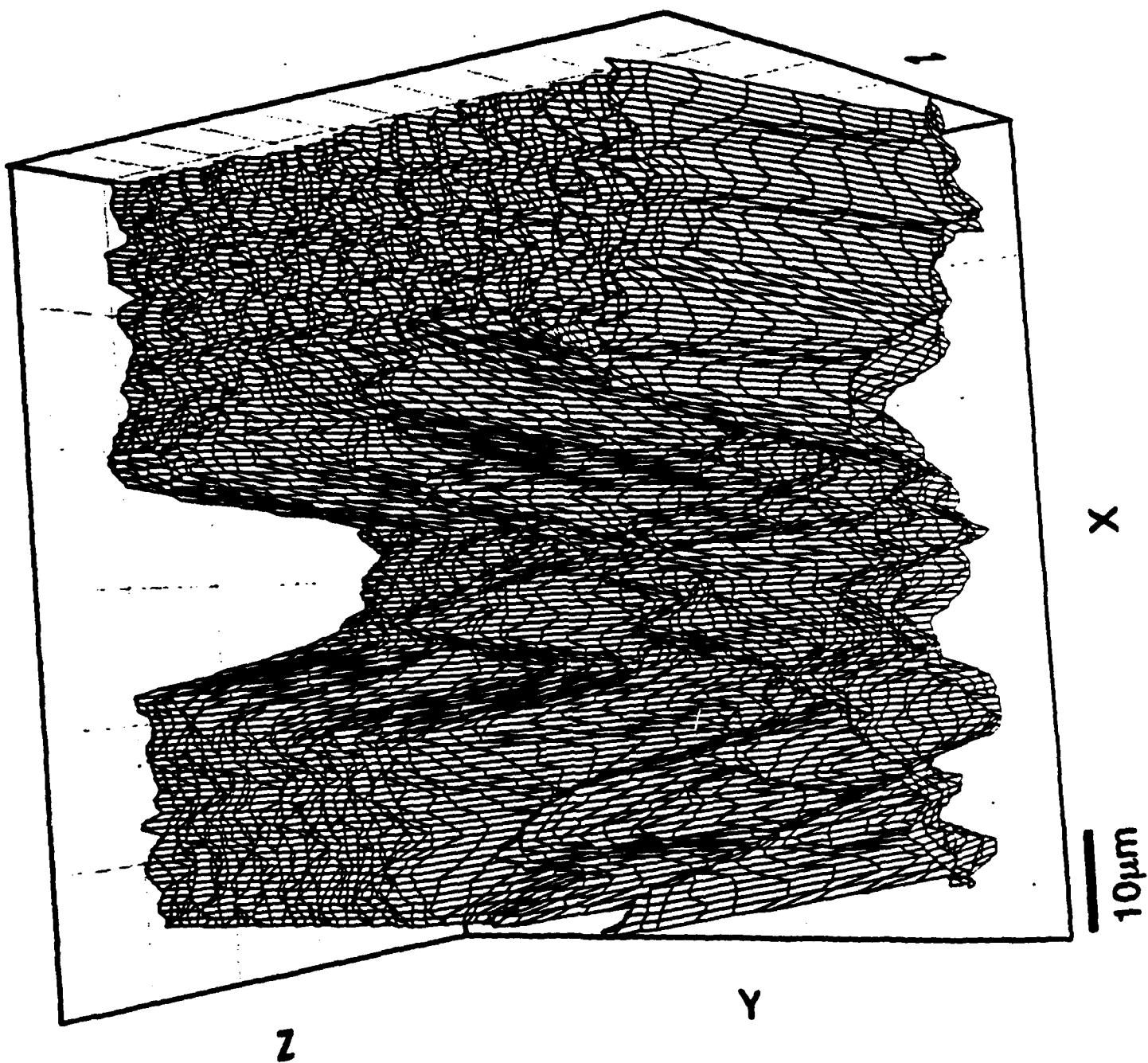


Fig. (4)

**A Coherent Hybrid Fiber-Optic Probe for Mapping  
Induced Birefringence in GaAs Structures**

**A Report by:**

**David L. Mazzoni, Kyuman Cho, and Christopher C. Davis**

**Optical Sensor Group**

**Electrical Engineering Department**

**University of Maryland**

**College Park, MD 20742**

**ph. (301) 405-3637**

**to be published in the Journal of Lightwave Technology**

**A Coherent Hybrid Fiber-Optic Probe for Mapping  
Induced Birefringence in GaAs Structures**

by

David L. Mazzoni, Kyuman Cho,\* and Christopher C. Davis

Electrical Engineering Department  
University of Maryland  
College Park, MD 20742  
ph. (301) 405-3637

**Abstract**

We report on a very sensitive fiber interferometric sensor for remote mapping of electro-optically induced birefringence in GaAs and other materials. This interferometer can be used to analyze and characterize GaAs structures without the need for elaborate testing equipment and procedures. The achieved spatial resolution is on the order of  $0.5\mu\text{m}$ .

---

\* current address: Department of Physics, Sogang University, 1 Sinsoo-Dong Mapo-Ku, Seoul, Korea

# **A Coherent Hybrid Fiber-Optic Probe for Mapping Induced Birefringence in GaAs Structures**

by

David L. Mazzoni, Kyuman Cho, and Christopher C. Davis

Electrical Engineering Department

University of Maryland

College Park, MD 20742

It is well known that GaAs has a large electro-optic (EO) coefficient. Therefore, GaAs integrated circuits and devices can be probed optically through the electro-optically induced birefringence produced by steady or transient voltages in the circuit. For example, Bloom et al. <sup>(1)</sup> have shown that noninvasive electro-optic sampling of microwave circuits is useful for measuring electrical waveforms propagating on a GaAs substrate. Previously, GaAs circuits had been tested by using a transmission line formed on an electro-optic substrate. EO crystals placed close to the device under test were sampled with a beam that probed the crystal to measure the fringing fields of the transmission line.<sup>(2)</sup> Unfortunately, this technique has limitations since the transmission line and crystal disturb the fields in the device under test. Techniques for non-perturbing, in-situ measurements, such as those investigated by Bloom, are more desirable since an external crystal is not required. We have extended the sensitivity and flexibility of electro-optic probing of GaAs structures through the use of a single-mode fiber probe that allows high resolution, remote mapping of induced birefringence in electro-optically active materials. These techniques allow us to map the local electric field in GaAs circuits. The electric field induced birefringence patterns mapped by the probe can be used to spatially monitor other parameters such as doping density, carrier concentration, etc. Also, we will show that this probe can be used

to uncover processing defects that would otherwise not be evident in conventional scanning electron microscope (SEM) imagery.

Induced birefringence can be monitored with high sensitivity by the use of coherent interferometry.<sup>(3)</sup> Typically in such experiments double beam interferometers such as the Mach-Zehnder are used in which two separate beams are derived from a single coherent source. The relative phase difference between these two beams can be detected by recombining them at a beam splitter and detecting concomitant intensity changes. The detection sensitivity of such arrangements is limited only by photon noise if a sufficiently coherent light source is used.

Practical, convenient interferometers can be built with fiber optic components, although better sensitivity can be obtained in a free space interferometer because an optical fiber is more susceptible to environmental noise. If two independent fiber arms are used in the interferometer, then local environmental disturbances will effect both fibers independently leading to increased background noise. In an optical fiber interferometer complete signal fading can also occur because of polarization state drift in the fiber. Optical fibers tend to be highly birefringent and small mechanical stresses, bending, and twisting of a fiber can induce linear and circular birefringence. The state of polarization (SOP) of a laser beam in such a fiber is subject to the induced birefringence. When the interferometer arms involve two independent fibers, the SOP's of returning beams may not be the same and complete signal fading can occur. However, an optical fiber interferometer does have several advantages: compact arrangements are possible, it does not require tedious alignment between measurements, and the probe light can be easily routed to the sample under test. Such versatility is essential for real time diagnostics.

Linear birefringence caused by the electro-optic effect can be measured coherently with a conventional interferometer. However, in order to minimize phase and polarization drifts that occur when independent signal and reference arms are used, we have combined two orthogonally polarized beams into a single fiber to minimize common-mode effects. The

birefringence of a GaAs sample will induce a phase shift between these orthogonally polarized beams where each polarization component can be regarded as belonging to an arm of a conventional interferometer. A polarization sensitive beam splitter can be used to demodulate the phase retardation on the beams. Since any fiber perturbation will affect both beams in the fiber, the system is relatively invulnerable to environmental effects, and common mode signals can be suppressed in the detection electronics. In addition, to avoid operating point drift that plagues synchronous detection schemes, we have used a true heterodyne scheme in which the two orthogonally polarized beams are at different frequencies.

A diagram of the fiber sensor is shown in Figure 1. A 35 mW  $1.3\mu\text{m}$  Nd:YAG laser is used as the signal source. A monolithic ring laser (Lightwave Technology Model 120-03) was chosen since it is recognized as an ideal light source for an interferometric sensor because of its narrow linewidth and small amplitude noise. GaAs is also transparent at the laser output wavelength of  $1.3\mu\text{m}$ . The beam is optically isolated and passes through a 40 MHz Acousto-Optic modulator (AOM) that produces two beams, one of which is shifted in frequency by 40 MHz from the fundamental. The plane of polarization of one of the beams is rotated  $90^\circ$  with respect to the other before entering polarizing beam splitter PSBS1. The two beams are combined in PSBS1 to yield two copropagating orthogonally polarized beams. These beams are injected into a single mode fiber and pass through a 3dB coupler. One of the coupler output beams is dumped into index matching fluid, while the other output beam continues to the sensing end. A 0.29 pitch graded index (GRIN) lens is epoxied to the end of the fiber with a focal point 5 mm from the GRIN lens. The GRIN is positioned above the GaAs sample at a height that gives maximum collection of the reflected beam. A computer controls an XYZ positioner that scans the GRIN above the GaAs device. The local electric field in the GaAs modulates the birefringence of the substrate and induces a phase shift between the orthogonal components of the probe beam. The beam is reflected back into the fiber and returns through the 3dB coupler, a  $\lambda/2$  waveplate, and polarizing

beam-splitter PSBS2 before reaching the detection photodiodes. The phase shift induced by the GaAs is detected by placing the output beam splitter (PSBS2) at  $45^\circ$  to the principal linear polarization directions, so that the two orthogonal components of the beam mix. Final detection occurs at a balanced mixer using two wideband photodiodes. Common mode amplitude noise is suppressed by differentially amplifying the signals from these two photodiodes.

The diode output currents in Fig.1 are

$$i_{1,2} \propto \frac{1}{2} \left[ |E_{\omega'}|^2 + |E_{\omega}|^2 \pm 2E_{\omega'}E_{\omega} \cos(\Delta\omega t + \phi_s - \phi_l) \right]. \quad (1)$$

The signals are combined in an RF differential amplifier to minimize amplitude noise, yielding

$$I_{diff} \propto \cos(\Delta\omega t + \Delta\phi_s - \phi_m), \quad (2).$$

where  $\Delta\omega = \omega - \omega'$  is the AOM excitation frequency,  $\phi_m$  is the induced phase shift, and  $\Delta\phi_s$  is the static phase term. Thus, the phase modulation on the optical carrier has been down converted to an RF frequency. The induced phase  $\phi_m$  can be detected by using standard RF demodulation techniques. Typically, in RF homodyne detection, a portion of the AOM drive is mixed with the detector output to beat the RF signal down to baseband. For optimum detection, this method requires active RF phase control to maintain quadrature ( $\Delta\phi_s = (2n + 1)\frac{\pi}{2}$ ) between the interferometer output and the AOM drive. Conversely, in RF heterodyne detection the sinusoidal signal modulation in  $\phi_m$  is directly detected in the phase locked loop (PLL) stage. The  $\Delta\phi_s$  term above represents a static phase shift due to differing path lengths, thermal expansion and contraction of the optical components, and other slowly varying effects. Heterodyne detection is immune to these pseudo-static phase perturbations since the PLL automatically tracks the static phase, unlike homodyne detection schemes. Furthermore, direct PLL detection does not require a stable source since the voltage controlled oscillator is locked to the carrier. Although other schemes exist for

heterodyne detection <sup>(4)</sup>, they often require complicated techniques and are usually not as sensitive as true heterodyne methods. <sup>(5)</sup>

The simplicity of the detection electronics using the direct PLL method is evident from Figure 1. The phase modulation is detected in a discrete 40 MHz PLL employing an automatic gain control (AGC) stage, doubly balanced mixer, 40 MHz VCO, and an active loop filter. Phase demodulation is achieved by mixing the differential amplifier output with the VCO output. The mixer output is filtered and is used to derive the VCO control voltage that keeps the VCO frequency and phase locked to the incoming RF carrier. The VCO control voltage also contains the demodulated phase signal, which is further amplified before the output signal is displayed on an oscilloscope or dynamic signal analyzer. This detection scheme is elegant and does not require any specialized or expensive components, making the sensor desirable for commercial applications.

GaAs belongs to symmetry group  $\bar{4}3m$ , so its linear electro-optic tensor is

$$r_{mk} = \begin{pmatrix} 0 & 0 & 0 \\ 0 & 0 & 0 \\ 0 & 0 & 0 \\ r_{41} & 0 & 0 \\ 0 & r_{41} & 0 \\ 0 & 0 & r_{41} \end{pmatrix}. \quad (3)$$

In a principal axis system the indicatrix is

$$\frac{x^2 + y^2 + z^2}{n_o^2} + 2r_{41}(E_x yz + E_y zx + E_z xy) = 1. \quad (4)$$

If the electric field is applied along the  $x$  direction, then

$$\frac{x^2 + y^2}{n_o^2} + 2r_{41}E_x yz = 1, \quad (5)$$

which has new principal axes  $y'$  and  $z'$  at  $45^\circ$  with respect to the original  $y$  and  $z$ . The corresponding indices are

$$n'_{y'} = n_o + \frac{1}{2}n_o^3 r_{41} E_x(x), \quad (6)$$

$$n'_z = n_o - \frac{1}{2}n_o^3 r_{41} E_z(x). \quad (7)$$

Therefore, only the  $x$  component of the electric field contributes to the birefringence. The resultant phase retardation for light after reflecting off the back surface of a GaAs sample is

$$\Gamma = \frac{2\pi}{\lambda} n_o^3 r_{41} V, \quad (8)$$

where  $V$  is the applied voltage.

The sensitivity can be calculated using Eq.(8). For example, when 5 Volts is applied to a wafer with a thickness of 500  $\mu\text{m}$ , the output signal is 45 dBV<sup>2</sup> above the noise floor in the spectrum analyzer trace. The unity SNR sensitivity calculated from these values after the spectrum analyzer bandwidth is taken into account is  $\simeq 20 \mu\text{rad}/\sqrt{\text{Hz}}$ . We have obtained sensitivities in this range using a similar interferometric arrangement with a He-Ne laser<sup>(3)</sup>.

We have tested several GaAs devices to prove the usefulness of the probe for detecting features that would otherwise not be evident. All samples were gold circuit patterns with mirrored ground planes deposited on (100) oriented substrates. With this orientation the probe beam travels in the vertical plane, which gives maximum sensitivity to the electro-optic effect. For example, we deliberately probed a test structure that had the SEM image shown on the left in Figure 2. The birefringence scan results on the right show that the gold features of the structure are exactly reproduced. The signal drops to zero on the gold features of the structure since the beam is reflected, and the maximum signal is observed adjacent to the gold features since the fringing field component in the  $z$  direction is maximum. Also, circuit features that could be overlooked in the SEM image stand out in the probe results. For example, there is a small gold stripe above and to the right of the alignment (+) mark. This can be clearly seen in the probe scan results and is barely discernible in the SEM image.

To prove the probe's usefulness as a diagnostic tool, a coplanar strip line was scanned. A

side view of the GaAs structure in Figure 3 shows the optical arrangement and GaAs crystal orientation. The structure has a mirrored gold coating on the back and gold circuit traces on the top surface. The birefringence of the underlying GaAs varies with distance from the surface traces due to the fringing fields that terminate on the ground plane underneath. The scan results are shown in Figure 4. However, there is a great deal of reproducible fine detail in the scan. This fine detail is *not* noise, but reflects real variation in the degree of local birefringence anisotropy. To demonstrate the reproducible nature of the fine structure in Figure 4, a high resolution scan of the circled region is shown as an inset. Fine variation of the birefringence anisotropy can result from inhomogeneities in doping density, crystal defects, failure to completely remove metal overlays during processing, or other processing defects. Fine variation in scans does *not* result from variation in the substrate thickness, since the signal from the probe depends on voltage acting across the substrate, not the local electric field. This shows that the probe can be used to obtain images showing general features followed by high resolution scans of the most interesting regions.

Another structure tested with the probe is shown in Figure 5. In this case the fringing electric field near gold features did not decay as expected, and there is a periodic structure evident in the results. This can be explained if there is any conducting pattern left on the substrate after processing. On further investigation we also noticed that the RF carrier level moved in anti-correlation to the detected phase shift. These observations can be explained if any of the  $p^+$  epi-layer remains after the processing steps. The carrier level would drop due to increased surface reflection in the epi-layer. However, the detected signal level increases when probing an epi-layer since the beam that penetrates sees a strong  $z$ -directed electric field. The presence of residual epi material would also explain why the electric field is maintained all the way to the edge of the substrate. It is important to note that an SEM image of the structure shows no observable features outside the gold stripes. We believe that such birefringence imagery can be useful in identifying potential problems in device processing and identifying subtle defects that affect device performance. Our

current spatial resolution is approximately  $0.5\ \mu\text{m}$ . This slightly better than diffraction limited resolution results from the effective confocal nature of the light delivery and re-collection by the single mode fiber. We anticipate even better resolution with tapered fiber tips.

This research is supported by the Department of Defense through Contracts DAMD17-90-Z-0052 and MDA904-91-C-9320.

### References

- [1] B. H. Kolner, D. M. Bloom, "Electro-optic sampling in GaAs integrated circuits", IEEE J. Quantum Electronics, **QE-22**, no.1, pp.79-93 January 1986.
- [2] B. H. Kolner, D. M. Bloom, and P. S. Cross, "Electro-optic sampling with picosecond resolution", Electron Lett., vol. 19, pp. 574-575, 1983
- [3] D. L. Mazzoni, K. Cho, C. C. Davis, "Hybrid fiber-optic sensor using true heterodyne measurement techniques", Optics Letters, **16** no.8 (April 1991)
- [4] T. Okoshi, "Polarization-state control schemes for heterodyne or homodyne optical fiber communications", IEEE J. Lightwave Technol., **LT-3** no.6. (December 1985).
- [5] I. M. I. Habbab, and L. J. Cimini, Jr., "Polarization-switching techniques for coherent optical communications", IEEE J. Lightwave Technol., **6-10**. (October 1988).

### Figure Captions

Figure 1. Experimental arrangement. In the figure: ISO - Optical Isolator, AOM - Acousto-Optic Modulator, PSBS - Polarization Sensitive Beam Splitter. SMF - Single Mode Fiber, VCO - Voltage Controlled Oscillator.

Figure 2. Birefringence probe scan result for a GaAs test structure with corresponding Scanning Electron Microscope (SEM) image on the left.

Figure 3. Side view of a GaAs coplanar strip line showing probe beam orientation and crystal orientation. Circuit traces on top are gold, and the polished bottom surface has a gold coating.

Figure 4. Birefringence probe scan result for a GaAs coplanar strip line structure. Fine details in the scan correspond to real features in the structure as is evident from high resolution scans of interesting areas ( inset ).

Figure 5. Birefringence probe scan result for test structure showing conductive pattern left on the substrate from an incomplete processing step.

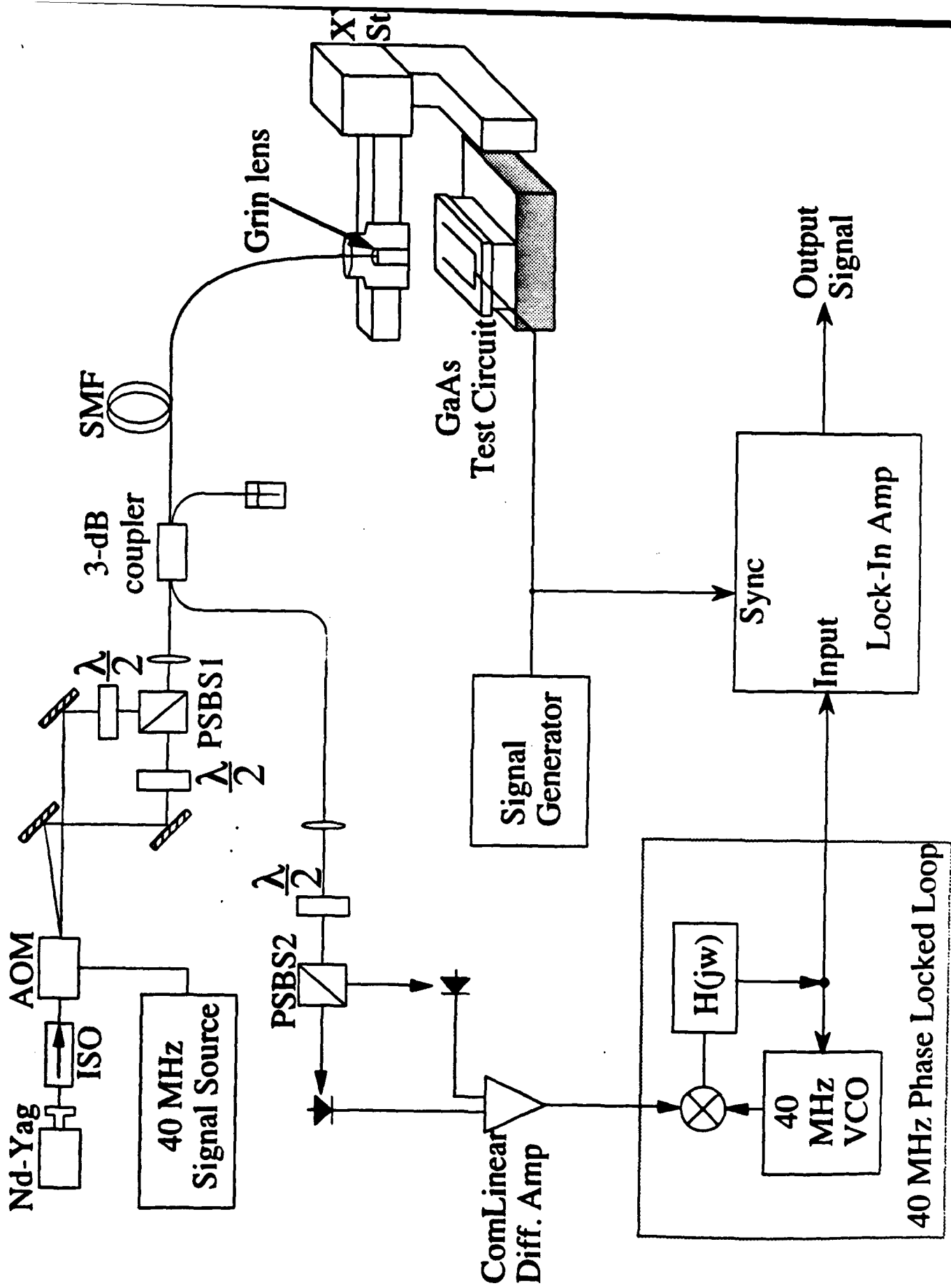


Fig.1

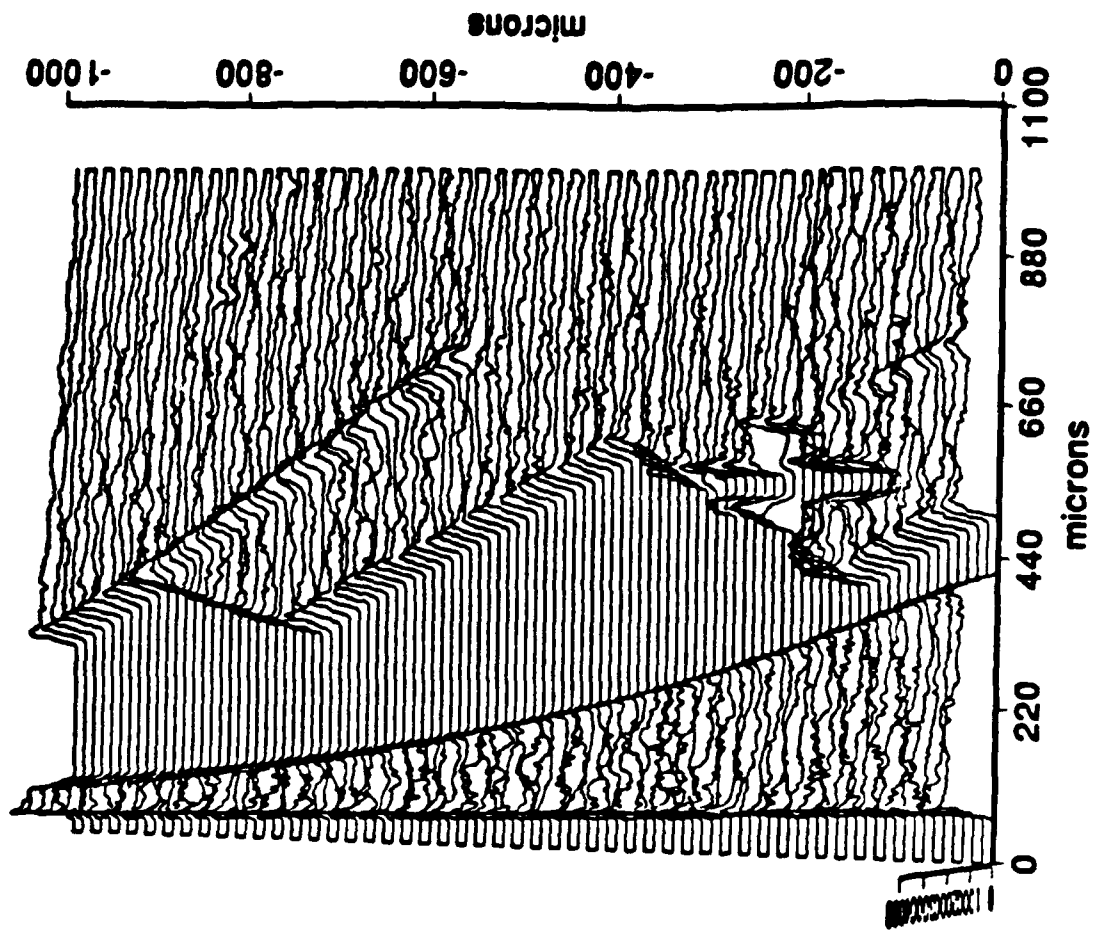
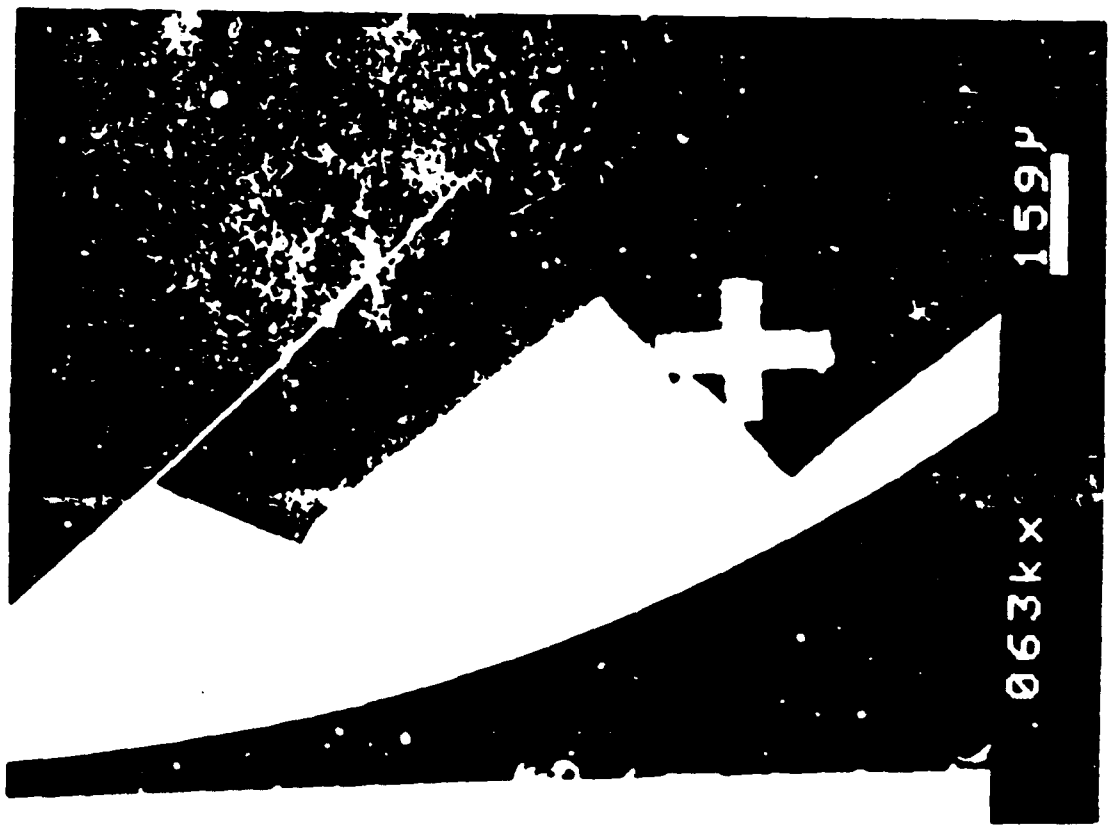


Fig.(2)

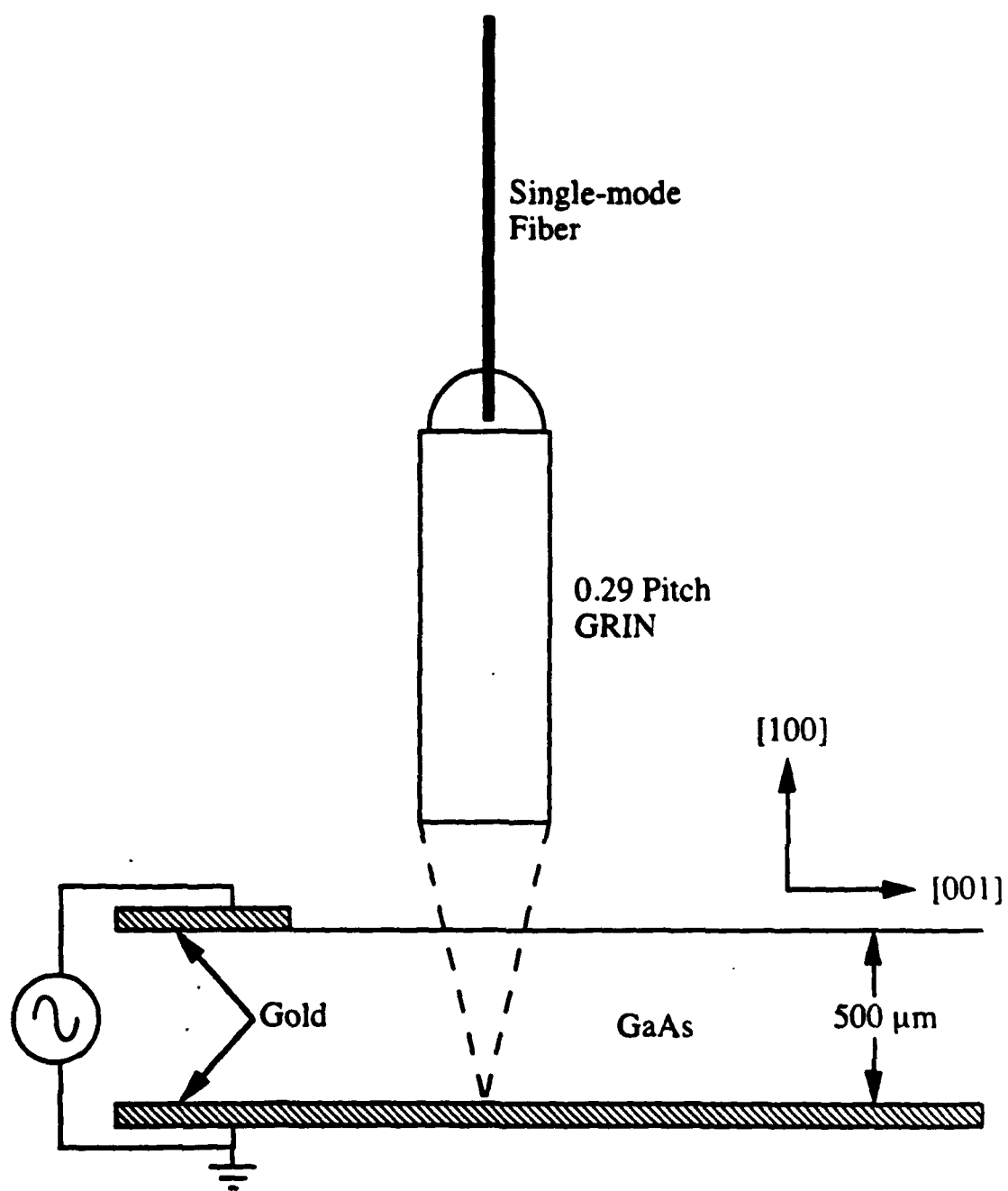


Fig. (3)

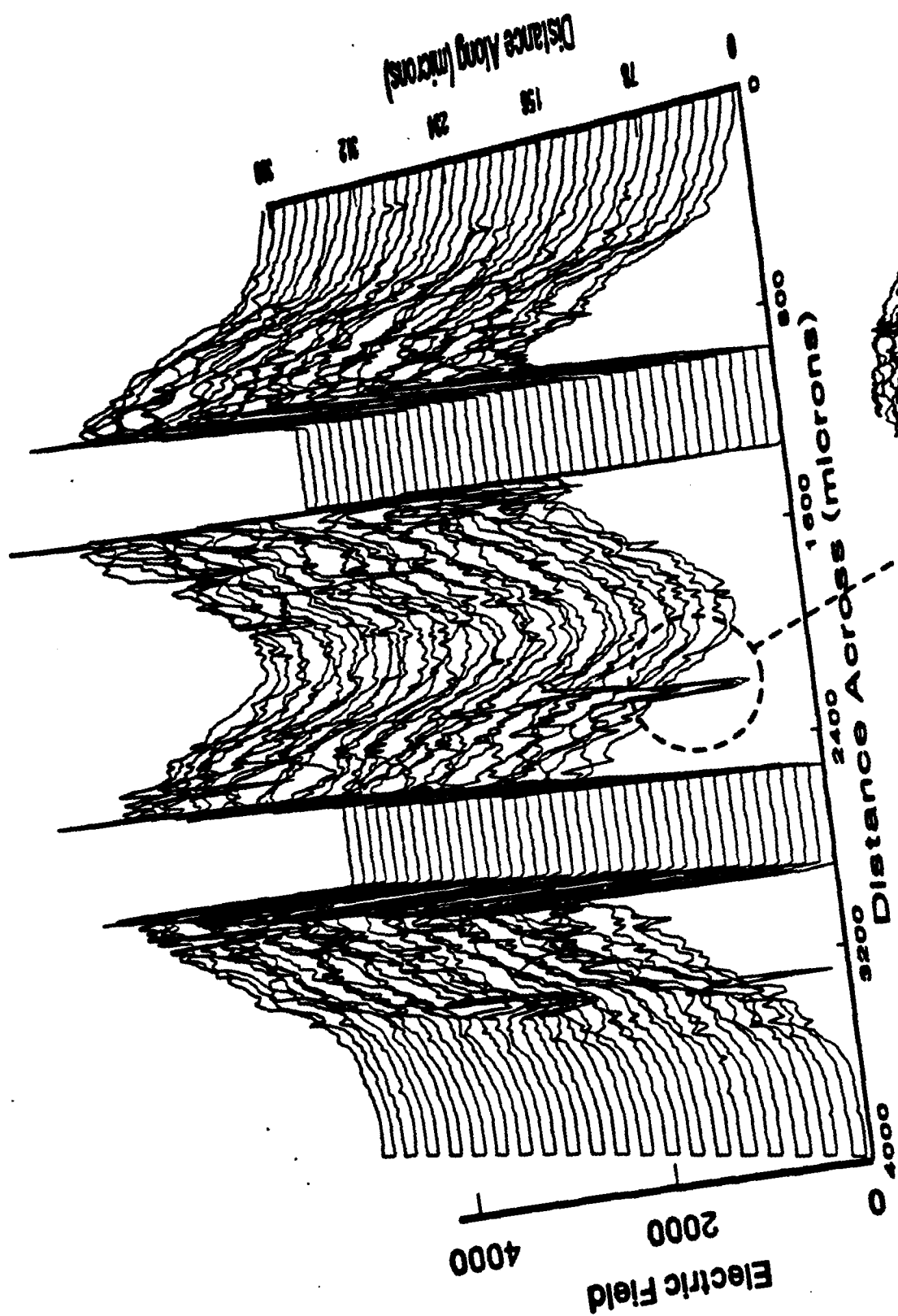


Fig. 4

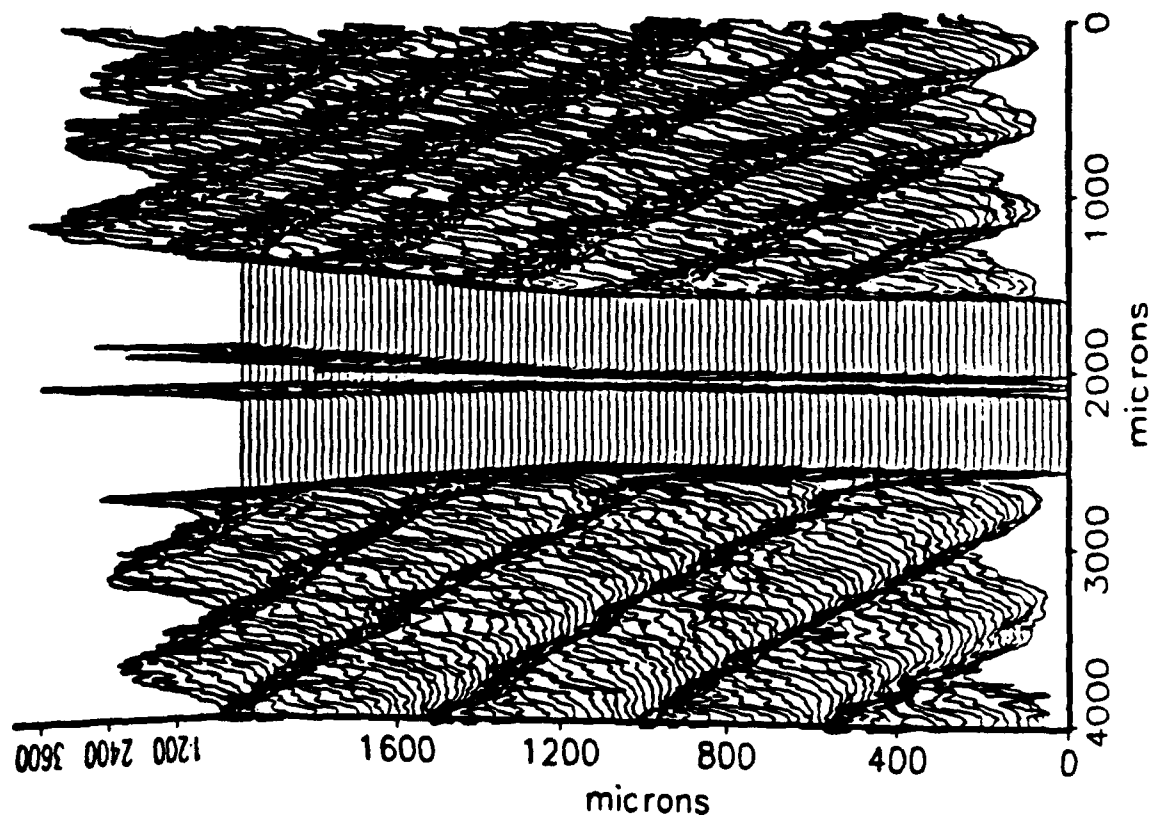


Fig. (5)